

# Cosmological Perturbation Theory and the Spherical Collapse model- I. Gaussian initial conditions.

Pablo Fosalba and Enrique Gaztañaga

*Institut d'Estudis Espacials de Catalunya, Research Unit (CSIC),  
Edf. Nerus-201 - c/ Gran Capità 2-4, 08034 Barcelona, Spain*

6 September 2021

## ABSTRACT

We present a simple and intuitive approximation for solving perturbation theory (PT) of small cosmic fluctuations. We consider only the spherically symmetric or monopole contribution to the PT integrals, which yields the exact result for tree-graphs (e.g. at leading order). We find that the non-linear evolution in Lagrangian space is then given by a simple *local* transformation over the initial conditions, although it is not local in Euler space. This transformation is found to be described the spherical collapse (SC) dynamics, as it is the exact solution in the shearless (and therefore local) approximation in Lagrangian space. Taking advantage of this property, it is straightforward to derive the one-point cumulants,  $\xi_J$ , for both the unsmoothed and smoothed density fields to *arbitrary* order in the perturbative regime. To leading order this reproduces, and provides with a simple explanation for, the exact results obtained by Bernardeau (1992, 1994). We then show that the SC model leads to accurate estimates for the next corrective terms when compared to the results derived in the exact perturbation theory making use of the loop calculations (Scoccimarro & Frieman 1996). The agreement is within a few per cent for the hierarchical ratios  $S_J = \xi_J / \xi_2^{J-1}$ . We compare our analytic results to N-body simulations, which turn out to be in very good agreement up to scales where  $\sigma \approx 1$ . A similar treatment is presented to estimate higher order corrections in the Zel'dovich approximation. These results represent a powerful and readily usable tool to produce analytical predictions to describe the gravitational clustering of large scale structure in the weakly non-linear regime.

**Key words:** cosmology:large-scale structure of Universe-cosmology: theory-galaxies: clustering-methods:analytical-methods: numerical.

## 1 INTRODUCTION

One of the important problems in Cosmology is the origin of galaxies, clusters, and structures seen on huge scales in the spatial distribution of galaxies and in the microwave background radiation. Given some initial seed fluctuations we would like to be able to make analytic predictions to describe the gravitational clustering that generates the large-scale structure that we see today.

The probability distribution function contains all the statistical information concerning the cosmic fields: density  $\delta$  and velocity  $v$  fluctuations. Here we will concentrate on its moments, the variance, skewness, kurtosis and so on. For a given set of moments in the initial conditions (IC), we would like to derive the final moments using the exact dynamics that rule the evolution of the underlying field. The problem is that the exact solution to the dynamical equations is only known for the linear regime of the evolution of these fields and only approximate solutions are known for their corre-

sponding non-linear stages. The spherical infall model has been used to provide a qualitative picture of how isolated (gravitationally bound) structures evolve up to their final collapse. In particular, the spherical model gives an estimation of when the first astrophysical objects formed purely under influence of gravity (see Peebles 1980, and references therein). This motivated the development of the so-called Press-Schechter formalism (Press & Schechter 1974) which gives the distribution of collapsed objects as a function of their mass. It is commonly assumed that highly non-linear objects such as galaxies form at peaks (*i.e.*, values above a threshold) of the underlying matter density field, what provides a possible mechanism for the segregation (*bias*) between luminous and dark matter in the universe (Kaiser 1984, Bardeen *et al.* 1986). More recently, Mo & White (1996) have extended the spherical collapse model to build a model for the spatial clustering of non-linear objects such as dark matter halos. Here we shall explain how the spherical

collapse model also appears in the context of Cosmological Perturbation Theory.

Cosmological Perturbation theory (PT) provides a framework to study small departures from linear theory: the weakly non-linear regime. The leading order contribution to the skewness for Gaussian initial conditions (GIC) was obtained by Peebles (1980). Fry (1984) extended this result to higher order moments and Bernardeau (1992, hereafter B92) found the generating function to the leading order contribution: the tree-level solution.

Comparison with observations and simulations made it necessary to develop PT for the smoothed fields. The smoothing corrections to the unsmoothed amplitudes for a power-law were first computed for the skewness for either a top-hat or a Gaussian window function by Juskiwicz *et al.* (1993). For a top-hat filter, Bernardeau 1994a (hereafter B94a) developed the machinery to systematically derive the smoothed hierarchical amplitudes for either the density ( $S_J$ ) or the velocity divergence ( $T_J$ ) fields to an arbitrary order (and arbitrary power spectrum). These results are in excellent agreement with numerical simulations (*e.g.*, Baugh, Gaztañaga, Efstathiou 1995, hereafter BGE95; Gaztañaga & Baugh 1995, Colombi *et al.* 1996). Work by Matsubara (1994) and Lokas *et al.* (1995) include some results for the Gaussian-smoothed density and velocity cumulants.

The success of the PT approach made it plausible to go further and study higher order (loop) corrections and the case of non-Gaussian initial conditions (NGIC). Despite the impressive achievements in the diagrammatic approach to loop corrections in PT by Scoccimarro & Frieman 1996a and 1996b, (hereafter SF96a and SF96b, respectively), the analytic entanglement faced when carrying out the calculations for the smoothed one-point cumulants is enormous. Moreover, regularization techniques must be used to evaluate the loop corrections through the kernels in Fourier space which, for a value of the spectral index  $n = -1$  lead to logarithmic divergences which become powers of the cut-off used in the regularization for  $n > -1$ . This puts constraints on the domain of applicability of the exact PT itself. When it comes to calculating the statistics of the smoothed fields, further analytic entanglement makes comparison with simulations and observations be restricted to few discrete values of the spectral index (Scoccimarro 1997, hereafter S97). For non-Gaussian initial conditions we have to face similar problems to start with, as loop corrections could enter at the same order than the tree-level contribution.

The general results derived by Bernardeau (B92, B94a and Bernardeau 1994b, hereafter B94b) show that the generating function follows the equation for the spherical collapse model. In this context this remarkable result lacked a satisfactory interpretation. What is the connection between PT and the spherical collapse model? Why does the generating function follow an equation for a fluctuating field? Why is the smoothed generating function given by the same unsmoothed result but with a different argument? Is this related to the Gaussian nature of the IC or the flatness of space? In this paper we will present a simple interpretation for these results, which will allow us to extend it to higher-order corrections and non-Gaussian initial conditions (NGIC).

This paper is organized as follows. We present the monopole approximation to PT in §2. In section §3 we give

a brief account of the estimation of the cumulants in PT and some of its nonlinear approximations. We investigate the Spherical Collapse (SC) model and its relation to PT in §4. In section §5 we present a comparison of the SC model with exact PT and N-body Simulations. General formulas for the one-point cumulants from a local transformation of the density field in *Lagrangian* space (for GIC) are provided in Appendix A. A comparison with analog results in *Euler* space is given in Appendix B. An alternative derivation of the smoothing effects in Fourier space for a top-hat window is illustrated in Appendix C. Further results are derived for the Spherically Symmetric Zel'dovich Approximation in Appendix D.

## 2 PERTURBATION THEORY AND THE MONOPOLE APPROXIMATION

We will now review briefly the main features of perturbation theory (PT) to present the spherical symmetric solution or monopole approximation. Throughout this paper we shall focus on Gaussian initial conditions and the Einstein-deSitter scenario (FRW with  $\Omega = 1$ ,  $\Lambda = 0$ ) to gain simplicity. However, a generalisation of the current approach to non-Gaussian IC and non-flat FRW universes will be provided in two accompanying papers (see Gaztañaga & Fosalba 1998, Fosalba & Gaztañaga 1998, Papers II & III, hereafter).

### 2.1 Equations of Motion

In a non-relativistic pressureless (collisionless) expanding universe, the field equations for the local fluctuation field  $\delta(x, t)$  in Euler space are:

$$\frac{\partial \delta}{\partial t} + \frac{1}{a} \nabla \cdot [(1 + \delta) \mathbf{v}] = 0 \quad (1)$$

$$\begin{aligned} \frac{\partial \mathbf{v}}{\partial t} + \frac{\dot{a}}{a} \mathbf{v} + \frac{1}{a} (\mathbf{v} \cdot \nabla) \cdot \mathbf{v} &= -\frac{1}{a} \nabla \phi \\ \nabla^2 \phi &= 4\pi G \bar{\rho} a^2 \delta \end{aligned} \quad (2)$$

which correspond to the mass conservation, Euler and Poisson equations respectively. The expansion factor  $a = a(t) \equiv (1 + z)^{-1}$  obeys:

$$\begin{aligned} \frac{\dot{a}}{a} &\equiv H = H_0 \left[ \Omega_0/a^3 + (1 - \Omega_0 - \Omega_\Lambda)/a^2 + \Omega_\Lambda \right]^{1/2} \\ \Omega_0 &= \frac{8\pi G \rho_0}{3H_0^2}; \quad \Omega_\Lambda = \frac{\Lambda}{3H_0^2}. \end{aligned} \quad (3)$$

Here  $H_0$  and  $\rho_0$  are the present values of the Hubble constant and background density, and  $\Lambda$  is the cosmological constant (see *e.g.*, Peebles 1980).

### 2.2 Perturbation Theory Solutions

A convenient approach to solve the field equations above is to expand the density contrast  $\delta$  assuming it is small as is usually done in the context of perturbation theory (PT) in Euler space,

$$\delta(\mathbf{x}, t) = \delta_1(\mathbf{x}, t) + \delta_2(\mathbf{x}, t) + \delta_3(\mathbf{x}, t) \dots, \quad (4)$$

were we assume that  $\delta_n \ll \delta_{n-1}$ . The first term  $\delta_1 \equiv \delta_l$  is the solution to the linearized field equations and is given in terms of the linear growth factor  $D(t)$ . The second term  $\delta_2 \sim \delta_l^2$  is the second-order solution, obtained by using the linear solution in the source terms, and so on.

The dominant mode to the linear PT solution,  $\delta_l$ , is given in terms of the linear growth factor  $D(t)$ :

$$\begin{aligned} \delta_l(x, t) &= D(t) \delta(x, 0) \\ D(t) &= \frac{\dot{a}}{a} \int_0^a da \, \dot{a}^{-3}, \end{aligned} \quad (5)$$

which for  $\Omega = 1$ , the so-called Einstein-deSitter universe, gives  $D(t) = a(t)$ . The linear approximation is therefore trivially local: *the evolution of a density fluctuation at a given point is not affected by its neighboring density fluctuations*, and all fluctuations grow with time at the same rate.

Beyond linear order, the equations of motion can be integrated for an Einstein-de Sitter universe, yielding for the growing mode (Peebles 1980),

$$\delta_2 = \frac{5}{7} \delta_l^2 + \delta_{l,\alpha} \Delta_{,\alpha} + \frac{2}{7} \Delta_{,\alpha\beta} \Delta_{,\alpha\beta} \quad (6)$$

where  $_{,\alpha}$  are partial space derivatives and we denote,  $\Delta(\mathbf{x}) = -4\pi \int d^3\mathbf{x}' \delta(\mathbf{x}')/|\mathbf{x} - \mathbf{x}'|$ .

The second order solution Eq.[6], explicitly shows that, although  $\delta_2$  is of order  $\delta_l^2$ , PT is formally *non-local* already at the second order as explicitly realized by the term accounting for the potential generated by the density fluctuations at different points ( $\sim \Delta$ ). In fact, the non-local nature of gravity is an intrinsic feature of General Relativity and remains so in the Newtonian limit through the tidal forces when the appropriate limit to the equations of motion is taken as was recently shown by Kofman & Pogosyan (1995).

To win simplicity in the equations of motion it is convenient to work in Fourier space:

$$\delta(\mathbf{k}) \equiv \frac{1}{V} \int d^3x \delta(\mathbf{x}) \exp(i\mathbf{k} \cdot \mathbf{x}), \quad (7)$$

so that one can formally write,  $\delta(\mathbf{k}) \equiv \sum_{n=1}^{\infty} \delta_n(\mathbf{k})$ , being  $\delta_n(\mathbf{k})$  the  $n$ -th order perturbative contribution. This is expressed as an  $n$ -dimensional integral over the kernels,  $F_n$ , that encode the non-linear coupling of modes due to the gravitational evolution,

$$\begin{aligned} \delta_n(\mathbf{k}) &= \int d^3q_1 \dots d^3q_n \delta_D(\mathbf{k} - \mathbf{q}_1 \dots - \mathbf{q}_n) \\ &\times F_n(\mathbf{q}_1 \dots \mathbf{q}_n) \delta_1(\mathbf{q}_1) \dots \delta_1(\mathbf{q}_n) \end{aligned} \quad (8)$$

where  $\delta_D$  is the Dirac function and the kernels  $F_n$  are given by symmetric homogeneous functions of  $\mathbf{q}_n$  with degree zero, that is, some geometrical average (see Fry 1984, Goroff *et al.* 1986, Jain & Bertschinger 1994, SF96a). In particular, for the second order we have:

$$F_2(\mathbf{q}_1, \mathbf{q}_2) = \frac{5}{7} + \frac{1}{2} \frac{\mathbf{q}_1 \cdot \mathbf{q}_2}{q_1 q_2} \left( \frac{q_1}{q_2} + \frac{q_2}{q_1} \right) + \frac{2}{7} \left( \frac{\mathbf{q}_1 \cdot \mathbf{q}_2}{q_1 q_2} \right)^2 \quad (9)$$

which reproduces Eq.[6] in Fourier space.

### 2.3 The Monopole Approximation

If we are in a situation where there is spherical symmetry we can substitute the kernels  $F_n$  in Eq.[8] by numbers  $\nu_n$ . This

numbers are given by the *monopole* term in an expansion of the kernels in spherical harmonics as they correspond to their angle averages (the outcome of the angular integrals in Eq.[24]). In other words, if we decompose the kernels,  $F_n$  in multipoles,

$$F_n(\mathbf{k}_1, \dots, \mathbf{k}_n) = F_n^{l=0} + \sum_{l=1}^{\infty} F_n^l, \quad (10)$$

only the first term  $F_n^{l=0}$ , the *monopole* (angle average of  $F_n$ ) which is the *spherically symmetric* contribution to the kernels, contributes to the Gaussian tree-level. We shall define, for convenience, the *monopole* in terms of some numbers  $\nu_n$  in the way,

$$F_n^{l=0} \equiv \langle F_n \rangle = \nu_n / n!, \quad (11)$$

where the factor  $n!$  reflects the fact that we are looking for some symmetric amplitudes. For instance, from Eq.[9] we have,

$$F_2^{l=0} \equiv \langle F_2 \rangle = \nu_2 / 2! = 34/21. \quad (12)$$

On the other hand, we can write the density fluctuation as formed of some generic *local* and *non-local* components,

$$\delta(\mathbf{x}) \equiv \delta^{loc}(\mathbf{x}) + \delta^{nloc}(\mathbf{x}) \quad (13)$$

where *local* means that the evolved (non-linear) density contrast at a given point is only a transformation of the linear density contrast at the same point, what we shall call a *local-density* transformation,  $\delta^{loc}(\mathbf{x}) = \mathcal{L}[\delta_1(\mathbf{x})]$ . The *non-local* component gives the contribution from density fluctuations at any other points. This is non-vanishing to all orders beyond the second in PT as commented above (see §2.2) since gravity induces a non-local (*i.e.*, non-isolated) evolution of the density fluctuations. The equivalent to this *local-density* transformation in Fourier space would then be,  $\delta^{loc}(\mathbf{k}) = \mathcal{L}[\delta_1(\mathbf{k})]$ . In particular, we can write the  $n$ -th perturbative order of  $\delta^{loc}(\mathbf{k})$  in the following way,

$$\delta_n^{loc}(\mathbf{k}) = \frac{c_n}{n!} \delta_l(\mathbf{k}) * \dots * \delta_l(\mathbf{k}) \quad (14)$$

which involves  $n$  convolutions of  $\delta_l(\mathbf{k})$ . By substituting  $F_n$  by its monopole contribution,  $\nu_n / n!$ , in Eq.[8], we immediately see that the above  $c_n$  numbers are just those given by the *monopole* term, *i.e.*,  $c_n = \nu_n$ . Transforming back to real space, we find  $\delta_n^{loc}(\mathbf{x}) = c_n / n! [\delta_l(\mathbf{x})]^n$ , and thus that *the monopole approximation is given by the local contribution to the density fluctuation* and has the form,

$$\delta^{loc}(\mathbf{x}) \equiv \sum_{n=1}^{\infty} \delta_n^{loc}(\mathbf{x}) = \mathcal{L}[\delta_1(\mathbf{x})] = \sum_{n=1}^{\infty} \frac{c_n}{n!} [\delta_l(\mathbf{x})]^n, \quad (15)$$

with  $c_1 = 1$ , to reproduce the linear solution. and  $c_n = \nu_n$  to recover the monopole.

### 3 CUMULANTS IN PERTURBATION THEORY AND OTHER APPROXIMATIONS

We will now show the connection between the tree-graphs in the diagrammatic approach to the one-point statistics and the *monopole* contribution to the kernels. This will allow us to use a simple local non-linear transformation (what we

shall call the *local-density* transformation) to derive the predictions for the cumulants in the perturbative regime from the *monopole* contribution alone.

### 3.1 Statistical Properties

The perturbative solutions above can be used to study the evolved statistical properties of the density fluctuations, which is our final goal. Here we concentrate on the  $J$ th-order moments of the fluctuating field:  $m_J \equiv \langle \delta^J \rangle$ . In this notation the variance is defined as:

$$\text{Var}(\delta) \equiv \sigma^2 \equiv m_2 - m_1^2 \quad (16)$$

In general, it is interesting to introduce the *connected moments*  $\xi_J$ , which carry statistical information independent of the lower order moments, and are formally denoted by a bracket with subscript  $c$ :

$$\xi_J \equiv \langle \delta^J \rangle_c \quad (17)$$

The connected moments are also called *cumulants*, *reduced moments* or *irreducible moments*. For a Gaussian distribution  $\xi_J = 0$  for  $J > 2$ . In many cases the higher order cumulants of a particular distribution are given in terms of the second order one  $\xi_2$ . It is therefore convenient to introduce some more definitions. A *dimensional scaling* of the higher order moments in terms of the second order one  $\xi_2 = \sigma^2$  is given by the following ratios:

$$B_J \equiv \frac{\xi_J}{\sigma^J} = \frac{\xi_J}{\xi_2^{J/2}} \quad (18)$$

We will see that for Gaussian initial conditions in perturbation theory, it is more useful to introduce the *hierarchical coefficients*,

$$S_J = \frac{\xi_J}{\xi_2^{J-1}}, \quad (19)$$

as PT predicts this quantities to be time-independent quantities on large scales. These amplitudes are also called normalized one-point cumulants or reduced cumulants. We shall also use *skewness*, for  $S_3$  and *kurtosis*, for  $S_4$ .

The way to proceed is to substitute the PT calculations Eq.[8] and commute the spatial integrals in  $\delta_n$  with the expectation values  $\langle \dots \rangle_c$ , by using the *fair sample hypothesis* (§30 Peebles 1980). Thus the calculation will reduce to averages over moments of  $\delta_1$  with the kernels in Eq.[8], which will, in turn, give us the statistical properties of  $\delta$  in term of the ones in the IC.

### 3.2 Linear Theory

If we only consider the first term in the PT series, Eq.[4], and the growing mode, Eq.[5], the cumulants of the evolved field will just be,  $\langle \delta^J \rangle_c = D^J \langle \delta_0^J \rangle_c$ , were  $\langle \delta_0^J \rangle_c$  correspond to the cumulants in the IC. Consistently, the hierarchical ratios (see Eq.[19]) will scale as,  $S_J = S_J(0)/D^{J-2}$ , were  $S_J(0)$  are the initial ratios. Note that this implies that the linear growth erases the initial hierarchical ratios, so that  $S_J \rightarrow 0$ , as time evolves (and  $D \rightarrow \infty$ ).

In terms of the dimensional scaling, see Eq.[18], we have,  $B_J = B_J(0)$ , so that the linear growth preserves the initial values. Note that if we want to do a meaningful calculation

of these ratios or the cumulants, in general, we might need to consider more terms in the perturbation series, Eq.[4], depending on the statistical properties of the IC, *e.g.*, how they scale with the initial variance, which is typically the smallness parameter in the expansion of the cumulants.

For GIC both  $B_J(0) = S_J(0) = 0$ , and we have to consider higher order terms in the perturbation series to be able to make a non-vanishing prediction.

### 3.3 The Tree-Level and Tree-Graphs

The computation of the cumulants in PT dates back to Peebles (1980) work where the leading order contribution to the skewness was obtained making use of the second-order PT as given in Eq.[6] to give,

$$S_3 \equiv \frac{\langle \delta^3 \rangle_c}{\langle \delta^2 \rangle_c^2} = \frac{34}{7} + \mathcal{O}[\sigma_l^2], \quad (20)$$

in agreement with the hierarchical scaling:  $\bar{\xi}_J \simeq \bar{\xi}_2^{J-1}$ . Fry (1984) extended Peebles analysis by making the connection between tree diagrams (or tree-graphs) and the perturbative contributions to leading order in the Gaussian case. With the help of this formalism he was able to obtain the leading order contributions for the three- and four-point functions making use of the 2nd and 3rd order in PT. Later on, Bernardeau (1992) found the generating function of the one-point cumulants to leading order for GIC. Furthermore, Fry (1984) found that, in general, the lowest order (tree-level) connected part that contributes to the  $J$ -order cumulant,  $\xi_J$ , is of order  $2(J-1)$  in  $\delta_1$  from terms like:

$$\langle \delta_1^2 \delta_2^{J-2} \rangle + \dots + \langle \delta_1^{J-1} \delta_{J-1} \rangle. \quad (21)$$

Note that this involves the cancellation of  $J-2$  contributions to the connected moment of order  $J$ . This is a property of the Gaussian initial conditions for which all  $\langle \delta_1^J \rangle_c$  vanish for  $J > 2$ . The above result Eq.[21] can be understood as follows. We are only interested in estimating the leading-order contribution (in terms of  $\delta_1$ ) to the connected part of the spatial average of the product  $\delta(\mathbf{k}_1)\delta(\mathbf{k}_2)\dots\delta(\mathbf{k}_n)$ , *e.g.*, that contribution made with terms that can not be factorized as products containing disjoint subsets of the labels. Each  $\delta$  is to be replaced with the perturbative expansion (see Eq.[4]), so that it may contain an arbitrary power in  $\delta_1$ . In the Gaussian case, the moments factorized only by pairs, so that the smaller contribution, with the smaller number of  $\delta_1$ , connecting  $J$  points has  $J-1$  pairs. Each pair corresponds to two  $\delta_1$  and therefore the leading contribution has indeed  $2(J-1)$  terms. These are the tree diagrams, corresponding to graphs with no loops (as any graph involving loops implies higher orders in  $\delta_1$ ). Therefore we see that for GIC the leading-order contribution to the cumulants (the so-called tree-level) is only made of tree diagrams (or tree graphs). That is why it is called the *tree-level*. We shall see in a companion paper (see Paper II) that the leading-order to the cumulants for non-Gaussian IC is not solely made of tree diagrams as there are additional terms which depend on the initial  $n$ -point correlation functions.

### 3.4 The Tree-Level and the Monopole Approximation

Consider a generic term of a tree-level contribution such as  $\langle \delta_n(\mathbf{k}_1)\delta_1(\mathbf{k}_2)\dots\delta_1(\mathbf{k}_{n-1}) \rangle$ . From Eq.[8] we have:

$$\begin{aligned} & \langle \delta_n(\mathbf{k}_1)\delta_1(\mathbf{k}_2)\dots\delta_1(\mathbf{k}_{n-1}) \rangle = \int d^3q_1\dots d^3q_n \\ & \times \delta_D(\mathbf{k}_1 - \mathbf{q}_1\dots - \mathbf{q}_n) F_n(\mathbf{q}_1\dots\mathbf{q}_n) \\ & \times \langle \delta_1(\mathbf{q}_1)\dots\delta_1(\mathbf{q}_n)\delta_1(\mathbf{k}_2)\dots\delta_1(\mathbf{k}_{n-1}) \rangle \end{aligned} \quad (22)$$

Thus we only have to perform the spatial integral over the initial moments  $\langle \delta_1^{2(n-1)} \rangle$ . In the case of GIC these moments are just products of two-point functions. The only terms in the products of two-point functions that produce *connected* graphs have pairs connected like:

$$\begin{aligned} & \int d^3q_1\dots d^3q_n \delta_D(\mathbf{k}_1 - \mathbf{q}_1\dots - \mathbf{q}_n) F_n(\mathbf{q}_1\dots\mathbf{q}_n) \\ & \times \langle \delta_1(\mathbf{q}_1)\delta_1(\mathbf{k}_2) \rangle \langle \delta_1(\mathbf{q}_2)\delta_1(\mathbf{k}_3) \rangle \dots \langle \delta_1(\mathbf{q}_n)\delta_1(\mathbf{k}_{n-1}) \rangle, \end{aligned} \quad (23)$$

*e.g.*, those terms with pairs of  $\mathbf{q}$  and  $\mathbf{k}$ , as otherwise there is a part of the integral that factorizes. By isotropy, one sees that the only dependence in the angles between the  $\mathbf{q}$ 's comes through  $F_n(\mathbf{q}_1\dots\mathbf{q}_n)$ . Thus, the geometrical dependence in Eq.[24] can be integrated out and the contribution of the kernels  $F_n$  just becomes a constant. Thus, *the (Gaussian) tree-level is given by the monopole and therefore by the local contribution to the density fluctuation* (see §2.3). As a result, in this scheme, the higher-order multipoles in the kernels are only expected to yield a non-vanishing contribution in the next-to-leading orders (loops) in the cumulants, while the monopole contributes to all perturbative orders. In what follows we shall deal with the *local* contribution to the density fluctuation alone,  $\delta_{loc}$  (monopole in the kernels) and work out its 1-point statistics.

### 3.5 Estimation of the Cumulants

We can now easily estimate *all* the 1-point statistical properties in the *monopole* approximation to PT. This can be done by using the generating function method:

$$\xi_J = \langle \delta^J \rangle_c = \left. \frac{d^J \ln[Z]}{dt^J} \right|_{t=0}, \quad (24)$$

where  $Z = \langle e^{t\delta} \rangle$  is the *moment generating functional* of the one-point probability distribution functional, and the field  $\delta \equiv \delta_{loc}$  is given by Eq.[15]. Furthermore,  $\ln[Z]$  is the *cumulant generating functional* so that Eq.[24] yields a simple derivation of the cumulants in terms of the moments. A general discussion in terms of the  $p$ -point correlation functions and its computation using diagrammatic techniques (similar to those in Quantum Field Theory) is given in detail in SF96a.

The resulting expressions can be found in Fry & Gaztañaga (1993, FG93 hereafter), who consider a generic local transformation between density fields and find, to leading terms in  $\sigma_l$ :

$$\begin{aligned} S_3 &= 3c_2 + \mathcal{O}(\sigma_l^2) \\ S_4 &= 4c_3 + 12c_2^2 + \mathcal{O}(\sigma_l^2) \\ S_5 &= 5c_4 + 60c_3c_2 + 60c_2^3 + \mathcal{O}(\sigma_l^2) \end{aligned} \quad (25)$$

for Gaussian initial conditions. Note that the leading contribution to  $S_J$  is enough to specify all the coefficients  $c_n$  in the transformation, and therefore all higher order corrections. As expected, by substituting  $c_2$  by the monopole contribution:  $c_2 = \nu_2$  in Eq.[12], one recovers Peebles (1980) calculation, Eq.[20].

### 3.6 The Local-Density Approximation and the Equations of Motion.

We shall stress that the *local-density transformation* (see Eq.[15]) is just a particular case of what is usually understood as *local*. In general, it means that the value of the evolved field at a given point is a transformation of the IC at the same point, say, the initial value of the field, its derivatives and any other fields (*e.g.*, the velocity field) contributing at that very point. Although gravity is non-local in this restricted sense, the above results show that the statistical average of the non-local integrals involved in the reduced moments to leading order are exactly given by a *local-density* transformation.

However, to estimate the leading order (tree-level) it is not necessary to calculate the full kernels  $F_n$ , as we only need the  $c_n$  numbers, the *monopole* (spherically symmetric) contribution. Therefore, *the values of  $c_n$  (and thus the appropriate local-density transformation) can be determined by finding the spherically symmetric solution to the equations of motion*. We shall see below that for the gravitational evolution of the density field in Lagrangian space, this transformation is given by the spherical collapse (SC) model, whereas for the ZA to the dynamics, it is given by what we shall call the Spherically Symmetric ZA (SSZA).

### 3.7 Other Approximations

In one dimension, the probability distribution function of the matter field may be integrated in Lagrangian coordinates making use of the Zel'dovich Approximation (ZA) which recovers the exact dynamics. For the three-dimensional case however, the ZA fails to describe the exact picture since the displacement field (that only depends on the IC) no longer factorizes in the actual solution for the growing mode as the ZA assumes (Bernardeau & Kofman 1995).

In the context of Lagrangian space and inspired by the successful results of the Zel'dovich Approximation (hereafter ZA), there have appeared in the last years a number of papers presenting some local approximations to the exact dynamics that successfully describe the evolution of the density contrast in its first non-linear stages (see Bertschinger and Jain 1994, Hui and Bertschinger 1996). Most recently, Protogeros and Scherrer (1997, hereafter PS97), following the formalism of the ZA, made use of a closed analytic expression,  $\delta = (1 - \delta_l/\alpha)^{-\alpha} - 1$ , to derive the cumulants following the formal analogy between the density contrast and the vertex generating function at tree level (see B92), for different values of  $\alpha$ , which they take to be different approximations to the exact PT. For the particular case when  $\alpha = 3$  (what they call the “spherical approximation”) their approximation happens to be equal to the spherically symmetric solution to the dynamics (in 3 dimensions) for the ZA (what we call SSZA in Appendix D). They also consider

the case  $\alpha = 3/2$  as another approximation they call the “exact approximation” (which, in fact, only reproduces the exact tree-level when  $\Omega = 0$ ). In general, none of these local approximations recovers the exact tree-level amplitudes as predicted by PT (which we will show later that is given by the SC model).

On the other hand, a number of non-local approximations to the non-linear dynamics of the cosmological fields have been designed as to simplify the equations of motion by linearising any of the fields involved. The Linear (or Frozen) Potential Approximation (LPA) which assumes that the gravitational potential generated by the density perturbations remains linear throughout the evolution (see Brainard *et al.* 1993, Bagla and Padmanabhan 1994), the Frozen Flow Approximation (FFA) that takes the velocity field to be frozen to its initial shape (see Matarrese *et al.* 1992), along with the ZA, which deals with the approximation that particles move on straight lines in the comoving picture (see Zel’dovich 1970), are the best known among them. A general treatment in terms of the vertex generating function can be found in Munshi *et al.* (1995). For a review of all these approximations see Bernardeau *et al.* (1994). If we write the second perturbative order as given by Eq.[6], in the generic form:

$$\delta = \delta_l + A \delta_l^2 + B \delta_{l,\alpha} \Delta_{,\alpha} + C \Delta_{,\alpha\beta} \Delta_{,\alpha\beta}, \quad (26)$$

one may derive the skewness at tree-level in the parametric fashion,

$$S_3 = 9A - 3B + 5C, \quad (27)$$

from which we can characterize the different above cited approximations depending on the weight each of them gives to these three different contributions: while PT gives  $A = 5/7$ ,  $B = 1$ ,  $C = 2/7$ , the ZA yields  $1/2$ ,  $1$ ,  $1/2$ , whereas the FFA gives  $1/2$ ,  $1/2$ ,  $0$ , and the LPA gets  $1/2$ ,  $7/10$ ,  $1/5$ , as the corresponding values for  $A$ ,  $B$  and  $C$  respectively, in each approximation. By just replacing the numbers in  $S_3$  one sees that none of these non-linear approximations is able to reproduce the exact tree-level amplitude given by PT for the skewness. This illustrates that, despite successfully describing the first non-linear stages of the gravitational collapse of a density fluctuation, none of the above given approximations yields to accurate enough predictions concerning the one-point cumulants in the perturbative regime.

### 3.8 Higher Perturbative Orders

Whenever  $\delta \lesssim 1$ , corrective terms beyond leading order (tree-level) become quantitatively important and must be taken into account. A systematic approach for deriving the next-to-leading orders in PT was introduced by Goroff *et al.* (1986) by representing them in terms of the *loop* diagrams. Recently, the first results for the *loop* corrections in PT have been calculated (see SF96a, SF96b and S97).

The angle averaged (spherically symmetric) picture described above can be used to estimate the *monopole* contribution to an arbitrary higher-order in PT. This is easy to do as one just has to take more terms in the series given by Eq.[15] to calculate the next orders in the moments. As expected, even in the Gaussian case, the higher-order terms coming from the monopole contribution differ from the exact PT estimates. Bernardeau (1994c, B94c hereafter) already

realised that fact when tracing the non-linear evolution of a volume occupied by particles that were in a given initial density perturbation. If one assumes that the matter content of a fluctuation is conserved during its collapse, then tracing the evolution of the volume is equivalent to following that of the matter density. In his work, the density fluctuation follows the SC model in what he called the *rare event limit*, i.e., when  $\delta_l/\sigma_l \rightarrow \infty$ , thus it is only exact as a mean picture of the actual collapse, with no scatter, i.e.  $\sigma_l = 0$ .

We have seen above that, in Fourier space, the departure of the SC picture from the exact PT is because the exact integrations in this case, e.g., such as that in Eq.[22] with more  $\delta_l$  factors, involve loops and the geometrical dependence is not trivial anymore (the dipole, quadrupole... contributions no longer cancel); The kernel  $F_n$  integration will give a different number depending on the loop configuration (see SF96a), contrary to the monopole approximation (were  $F_n$  is always replaced by the same amplitude  $c_n/n!$ ). However, one can naively expect the monopole contribution to dominate by symmetry because asymmetric contributions (arising from tidal terms) tend to cancel when averaged. In this paper we shall compute the monopole contribution to PT and will compare it to the exact analytic results, when available, or N-body simulations, to see how accurate this approximation is.

## 4 THE SPHERICAL COLLAPSE MODEL

### 4.1 The Shearless Approximation in Lagrangian Space

We next want to derive the evolution of a density fluctuation within the spherical model of collapse. In order to do that, we turn to the Lagrangian space which is the natural framework for describing the motion of a fluid element. The SC dynamics is fully described in terms of one parameter, the initial size of the spherical fluctuation. In this sense, the SC model is just a particular case within the family of *local-density* approximations discussed above. When we write the equations in Lagrangian space, the natural variable is the density contrast and the only parameter in terms of which the solution is given is the linear density contrast.

We first must define the conformal time  $\tau$  which is the comoving time parameter to the motion of the mass and we shall denote with a dot the associated time derivatives (conformal time derivatives), defined as,

$$\frac{d}{d\tau} = \frac{\partial}{\partial\tau} + \mathbf{v} \cdot \nabla_q \equiv a(t) \frac{d}{dt}, \quad (28)$$

$a(t)$  being the scale factor. The generic equation describing the evolution of a spherically symmetric perturbation in an expanding universe is given by,

$$\frac{d^2 R}{dt^2} = -\frac{GM(R)}{R^2} = -4\pi G \rho R \quad (29)$$

since the matter contained in a spherical perturbation of radius  $R$  is,  $M(R) = 4\pi\rho R^3/3$ . Therefore, the spherical density perturbation  $\delta = (R/a(t)R_0)^{-3} - 1$ , is described by the following equation of motion

$$\ddot{\delta} + \mathcal{H}(\tau)\dot{\delta} - \frac{4}{3} \frac{\delta^2}{(1+\delta)} = 4\pi G(\rho - \bar{\rho})a(\tau)^2(1+\delta). \quad (30)$$

where the dot denotes a conformal time derivative, and  $a(\tau)$  is the scale factor in terms of the conformal time from which we define the conformal Hubble parameter  $\mathcal{H}(\tau) = d \log a(\tau)/d\tau$ . Introducing the comoving time derivative,  $d/dt \equiv \cdot$ , the last equation translates into,

$$\ddot{\delta} + 2H(t)\dot{\delta} - \frac{4}{3} \frac{\dot{\delta}^2}{(1+\delta)} = 4\pi G\bar{\rho}\delta(1+\delta), \quad (31)$$

where  $H(t) = d \log a(t)/dt$ .

On the other hand, the Newtonian Fluid equations with zero pressure, which are the appropriate description for the sub-horizon modes in a perturbed FRW universe, in its matter dominated regime (the relevant for describing formation of structures), are usually given in Euler space (see *e.g.*, §9 in Peebles 1980). If we now turn to *Lagrangian* coordinates and we re-express the equations of motion in terms of the derivatives of the conformal time  $\tau$ , the continuity equation reads,

$$\dot{\delta} + (1+\delta)\theta = 0, \quad \theta \equiv \nabla \cdot \mathbf{v}. \quad (32)$$

We then combine this last expression with the Raychaudhuri equation,

$$\dot{\theta} + \mathcal{H}(\tau)\theta + \frac{1}{3}\theta^2 + \sigma^{ij}\sigma_{ij} - 2\omega^2 = -4\pi G\bar{\rho}\delta a^2 \quad (33)$$

where  $\omega^2 \equiv \frac{1}{2}\omega^{ij}\omega_{ij}$ , and the expansion  $\theta$ , vorticity  $\omega_{ij}$ , and shear  $\sigma_{ij}$ , are given by the trace, traceless antisymmetric and symmetric parts respectively, of the velocity divergence,

$$\begin{aligned} \nabla_i v_j &= \frac{1}{3}\theta\delta_{ij} + \sigma_{ij} + \omega_{ij}, \\ \sigma_{ij} &= \sigma_{ji}, \quad \omega_{ij} = -\omega_{ji}, \end{aligned} \quad (34)$$

and get a second-order differential equation for the density contrast,

$$\begin{aligned} \ddot{\delta} + \mathcal{H}(\tau)\dot{\delta} - \frac{4}{3} \frac{\dot{\delta}^2}{(1+\delta)} \\ = (1+\delta) \left( \sigma^{ij}\sigma_{ij} - 2\omega^2 + 4\pi G\bar{\rho}\delta a^2 \right). \end{aligned} \quad (35)$$

For an initially irrotational fluid (the expansion preserving its irrotational character in the linear regime):  $\omega = 0$ . Making the further assumption that there is *no shear*, Eq.[35] leads to the equation we obtained for the SC model (see Eq.[30] above). In other words, *the SC approximation is the actual dynamics when tidal effects are neglected*. As one would expect, this yields a *local* evolution, in the restricted sense that the evolved field at a point is just given by a local (non-linear) transformation of the initial field at the same point. Throughout this paper we shall drop the shear term and work out the solution to this dynamics in the perturbative regime.

The exact (non-perturbative) solution for the SC of the density contrast in an Einstein-deSitter universe admits a well-known parametric representation,

$$\delta(\phi) = \frac{9}{2} \frac{(\phi - \sin \phi)^2}{(1 - \cos \phi)^3} - 1, \quad \delta_l(\phi) = \frac{3}{5} \left[ \frac{3}{4}(\phi - \sin \phi) \right]^{2/3}$$

for  $\delta_l > 0$ , linear overdensity, and

$$\delta(\phi) = \frac{9}{2} \frac{(\sinh \phi - \phi)^2}{(\cosh \phi - 1)^3} - 1, \quad \delta_l(\phi) = -\frac{3}{5} \left[ \frac{3}{4}(\sinh \phi - \phi) \right]^{2/3},$$

for  $\delta_l < 0$ , linear underdensity (see Peebles 1980), where the

parameter  $\phi$  is just a parameterization of the time coordinate.

If we are only interested in the perturbative regime ( $\delta_l \rightarrow 0$ ), which is the relevant one for the description of structure formation on large scales, the above solution can be also expressed directly in terms of the initial density contrast, which plays the role of the initial size of the spherical fluctuation in Eq.[31]. This way, the evolved density contrast in the perturbative regime is given by a *local-density* transformation of the linear density fluctuation,

$$\delta = f(\delta_l) = \sum_{n=1}^{\infty} \frac{\nu_n}{n!} [\delta_l]^n \quad (36)$$

Notice that all the dynamical information in the SC model is encoded in the  $\nu_n$  coefficients of this *local-density transformation*, Eq.[36]. In an Einstein-de Sitter universe ( $\Omega = 1, \Lambda = 0$  FRW universe), we can introduce the above power series expansion in Eq.[31] and determine the  $\nu_n$  coefficients one by one. The first ones turn out to be,

$$\begin{aligned} \nu_2 &= \frac{34}{21} \sim 1.62; \quad \nu_3 = \frac{682}{189} \sim 3.61 \\ \nu_4 &= \frac{446440}{43659} \sim 10.22; \quad \nu_5 = \frac{8546480}{243243} \sim 35.13 \end{aligned} \quad (37)$$

and so on.

Remember that this evolution is in *Lagrangian* space,  $\delta = \delta(\mathbf{q})$ . We would like to relate the above results, obtained in Lagrangian coordinates to the corresponding fluctuation in Eulerian coordinates. In Lagrangian space a fluid element of a given mass is labeled by its initial position  $\mathbf{q}$  (or Lagrangian coordinate), whereas Eulerian space uses the density  $\rho(\mathbf{x})$  at the final coordinate  $\mathbf{x} = \mathbf{x}(\mathbf{q})$ . Notice that mass conservation requires that the volume elements be related like:  $d^3\mathbf{q} = (1+\delta)d^3\mathbf{x}$ . Thus density probabilities in Lagrangian ( $L$ ) and Eulerian ( $E$ ) space should also be related by the same factor,  $\Delta_L\delta = (1+\delta)\Delta_E\delta$  (see Kofman *et al.* 1994). This provides a simple way to translate density moments in Eulerian space,  $\langle (1+\delta)^J \rangle_E$  with the ones in Lagrangian space  $\langle (1+\delta)^J \rangle_L$ ,

$$\begin{aligned} \langle (1+\delta)^J \rangle_L &= \int (1+\delta)^J P[\delta] \Delta_L \delta = \\ &= \int (1+\delta)^{J+1} P[\delta] \Delta_E \delta = \langle (1+\delta)^{J+1} \rangle_E. \end{aligned} \quad (38)$$

In particular, as pointed out by Bernardeau (B94b) (and also PS97), the conservation of Eulerian volume yields,  $\langle 1 \rangle_E = 1 = \langle (1+\delta)^{-1} \rangle_L$ , which requires a normalization for  $\delta$  in Eq.[36]:

$$1 + \delta = (1 + f) \langle (1 + f)^{-1} \rangle_L. \quad (39)$$

It is interesting to note from Eq.[38] that:

$$\langle \delta^J \rangle_L = \langle \delta^J \rangle_E + \langle \delta^{J+1} \rangle_E. \quad (40)$$

Thus, to leading order, there is no difference between Eulerian and Lagrangian moments. In general, the leading contribution to the cumulants is enough to specify all the coefficients  $c_n$  (see *e.g.*, Eq.[25]), of the local transformation provided by Eq.[15]. This means that the local-density transformations that produce the tree-level in PT are identical in Euler and Lagrangian space. A similar result was noted by Protogeros & Scherrer (PS97), in the context of hierarchical

distributions, but this argument is more general as applies to any non-Gaussian distributions where:  $\langle \delta^{J+1} \rangle_E < \langle \delta^J \rangle_E$ , which holds even for the strongly non-Gaussian dimensional models, Eq.[18], that we shall investigate later (see Paper II). These models for the IC naturally appear as solutions for the topological defects models for structure formation.

#### 4.2 The SC as a Solution to the Cumulants

Our goal here is to relate the cumulants of the initial distribution with the ones resulting from the full non-linear evolution of the field. To estimate the evolved cumulants under the SC model, we perform the following prescription:

- (a) we start with the initial cumulants, in the limit of small fluctuations,  $\delta \rightarrow 0$ . In this limit, the cumulants are equal in Lagrangian and Eulerian space, as  $d^3\mathbf{q} \rightarrow d^3\mathbf{x}$ .
- (b) we then use the local transformation Eq.[36], with its proper normalization, Eq.[39], to relate the initial and final cumulants in Lagrangian space. As argued above, this is equivalent to include the contribution from the monopole alone. This can be done as described in section §3.5 using Eq.[24] to obtain expressions such as Eq.[25] by keeping the relevant terms.
- (c) finally we use Eq.[38] to relate the Lagrangian and Eulerian moments, which can be rewritten in a more compact way:

$$\langle \delta^J \rangle_E = \langle \delta^{J-1} \rangle_L - \langle \delta^{J-2} \rangle_L + \langle \delta^{J-3} \rangle_L - \dots + \langle \delta \rangle_L, \quad (41)$$

from which we get the cumulants in Euler (real) space.

Note that the cumulants obtained from (b)+(c), which are Appendix A (see Eq.[A2]), are not the same as the ones obtained using the local-density relation in *Euler* space directly (see Appendix B). As explicitly seen from Eq.[40], they are only the same to leading order. We choose this approach because the Lagrangian space, comoving with the fluid element, is the natural coordinate system for a local description of its evolution. Note that a local-density description in Lagrangian space will in general mean a non-local one in Euler space.

#### 4.3 The SC Model and PT

We have pointed out in the previous sections that the monopole contribution (which is the exact result for tree-graphs) to the cumulants in PT is given by a local-density transformation Eq.[15], whose coefficients,  $c_n$ , are to be determined by the kernels,  $F_n$  (see Eq.[8]), under the relevant dynamics. These arguments are valid for any dynamics and apply either to Euler or Lagrangian space. They are true for any leading order calculation. As argued in section §3.6, to estimate this contribution to the cumulants it is not necessary to calculate the full kernels  $F_n$ , as we only need the numbers  $c_n$ . Given the equations for the evolution of a field, one can determine Eq.[15] and therefore  $c_n$  by just requiring the solutions to be *spherically symmetric*.

We have shown above that for gravity, the spherically symmetric solution to the evolution of density perturbations is given by Eq.[30], *e.g.*, the SC model, whose solution is well-known (see Eq.[36]). Thus,  $\mathcal{L} = f$  which yields the

monopole contribution,  $c_n = \nu_n$ , without need of estimating the kernels  $F_n$  or any integral. Note, in particular, that  $\nu_2 = 34/42$  from both approaches (see Eqs.[12],[37]).

This provides with a simpler derivation and interpretation of the results presented by B92, who found the values  $\nu_n$  that give the leading-order contribution to PT for Gaussian initial conditions. In the language of B92, the vertex generating function,  $\mathcal{G}(-\tau) = f(\delta_i)$  (see also PS97). Our derivation explains therefore why the vertex generating function  $\mathcal{G}(-\tau)$  follows the SC model, which lacked a satisfactory explanation in the context of B92. Besides its simplicity, in our framework one has the added advantage of being able to use the local-density relation to estimate the higher-order corrections for both Gaussian and non-Gaussian initial conditions (see Paper II). Note nevertheless that there is an important difference in practice with the work of B92. His vertex generating function  $\mathcal{G}(-\tau)$ , corresponds to cumulants in Euler space, while our local-density relation  $f(\delta_i)$ , applies to Lagrangian space. To leading order, both give identical results for Gaussian IC, but they yield different results in general for Non-Gaussian IC or for next-to-leading terms for Gaussian IC.

We want to stress that the fact the SC model determines the tree-level amplitudes is neither a singular property of the Gaussian nature of the IC nor an argument that has to do with the flat geometry of space. It is a general property that follows straightforwardly from the *local* nature of the monopole contribution to PT (see section §3.6): *the tree-graphs (and the monopole contribution) in PT are exactly given by the SC model regardless of either the statistical nature of the initial conditions or the geometry of the universe*. We shall illustrate the above statement in the framework of B92 calculations by showing, in an accompanying paper (Fosalba & Gaztañaga 1998, Paper III in this issue), that the equations of motion that govern the leading order amplitudes (for Gaussian initial conditions) in a universe with arbitrary density parameter  $\Omega$ , are those of the SC dynamics.

#### 4.4 Smoothing Effects

So far we have worked out the statistics of the unsmoothed fields. There remains to be seen whether the local-density approximation may be extended to the statistics of the spatially smoothed fields, which is essential if we are to compare with N-body simulations and observations. For that purpose, we have to introduce the fluctuating field integrated over a *finite* volume. This volume is fixed by the size of the window function that acts as a filter on the unsmoothed field.

Our goal is therefore to relate the *smoothed* cumulants in the evolved distribution with the *smoothed* cumulants in the initial one. The latter are *inputs* to our calculations and should tell us, *e.g.*, how the smoothed *rms* fluctuation changes as a function of the smoothing radius:  $\hat{\sigma} = \hat{\sigma}(R)$ .

We will focus here in the top-hat filter, defined as,

$$W_{TH}(\mathbf{x}, R) = 1 \quad \text{if} \quad \mathbf{x} \leq R,$$

being zero otherwise, where  $R$  is the smoothing radius. Note that this filter is spherically symmetric so that the transformation that gets from the unsmoothed to the smoothed evolved fields preserves the spherical symmetry.



In the local-density picture of the spherical collapse, each fluctuation is isolated from the others and evolves according to the value of the initial amplitude alone. The statistics of the evolved field is just induced by the statistics of the initial one, which could in general be non-Gaussian. In order to estimate the statistical properties (one-point cumulants) we can therefore picture the initial spatial distribution as just made of a single spherical fluctuation. Different realizations of this fluctuation could have different amplitudes or shapes in a proportion given so as to match the statistics of the initial conditions (see §61 Peebles 1980 for examples). In our case this is given in terms of the *unsmoothed* distribution, which corresponds to a top-hat smoothing of radius  $R_0 \rightarrow 0$ .

The spatial smoothing only acts on the fluctuation by changing its amplitude. We want, by construction, the new amplitude to be a function of the smoothing radius,  $R$ . Thus, for the initial conditions  $\delta_l$ , the smoothed field is:

$$\hat{\delta}_l(R) = \frac{\hat{\sigma}_l(R)}{\sigma_l(R_0)} \delta_l \quad (42)$$

as smoothing does not change the statistics directly (at least for a top-hat). A similar argument applies to the evolved field, which under the SC model is just a local transformation of the initial fluctuations, which only changes the local amplitude:

$$\hat{\delta} = \frac{\hat{\sigma}}{\sigma} \delta \quad (43)$$

where  $\hat{\delta}$  is the smoothed fluctuation and  $\delta$  the unsmoothed one. The statistics of  $\hat{\delta}$  will therefore be given by the unsmoothed statistics,  $\delta$ , which are in turn given by the local-density relation Eq.[36]:  $\hat{\delta} \sim \delta = f[\delta_l]$ . Using Eq.[42] we express this as a function of the linear smoothed fluctuation  $\hat{\delta}_l$ :

$$\hat{\delta}[\hat{\delta}_l] \sim f[\hat{\delta}_l \frac{\sigma_l}{\sigma_l}] \quad (44)$$

where  $\sim$  just means that  $\hat{\delta}$  needs to be normalized, as explained before (see Eq.[39]). Note that the input *rms* fluctuation is a function of the smoothing radius,  $R$ , which also fixes the amplitude of the final smoothed fluctuation. As the smoothing radius  $R$  is, by construction, larger than the unsmoothed one  $R \gg R_0 \rightarrow 0$ , we have for the smoothed fluctuation:  $\hat{\rho} = \frac{\hat{\sigma}}{\sigma} \sim m_0 R^{-3}$ , as there is no other smoothing than the sharp cut-off, (note that this may not be the case for other filters, such as the Gaussian smoothing, which changes the initial shape of the fluctuation and therefore the final mass). Thus the smoothed amplitude,  $\hat{\sigma} = \hat{\sigma}[R]$ , will be a function of  $\hat{\delta}$  through  $R$ . This together with Eq.[44] can be used to obtained  $\hat{\delta}$  in a recursive way.

In the case of a power-law power spectrum  $P(k) \sim k^n$ , the smoothed variance is also a power-law  $\hat{\sigma}_l \sim R^{\gamma/2}$ , where  $\gamma = -(n+3)$ . We then have,  $\hat{\sigma}_l = \sigma_l (1 + \hat{\delta})^{-\gamma/6}$ . Note that  $\gamma = 0$  reproduces the unsmoothed result. Moreover, using Eq.[44], we find:

$$\hat{\delta}[\hat{\delta}_l] \sim f[\hat{\delta}_l (1 + \hat{\delta})^{\gamma/6}] \quad (45)$$

up to a normalization factor given by Eq.[39]. Note that this final result as well as the general expression Eq.[44], agrees with B94a arguments, based on the vertex generating function. However, Eqs.[44],[45] do not limit themselves to Gaussian initial conditions or the leading-order term. Here again,

the vertex generating function  $\mathcal{G}(-\tau)$ , corresponds to cumulants in Euler space, while our local-density relation,  $f(\delta_l)$ , applies to *Lagrangian* space. To leading order, they both give identical results with Gaussian IC, but they yield different results, in general, for Non-Gaussian IC or for higher-order terms with Gaussian IC.

We will further write the smoothed density contrast (over a smoothing scale  $R$ ) in the following way:

$$\hat{\delta} = f(\hat{\delta}_l) \equiv \sum_{k=1}^{\infty} \frac{\overline{\nu}_k}{k!} [\hat{\delta}_l]^k, \quad (46)$$

where the  $\overline{\nu}_k$  are a generalization of the unsmoothed coefficients. By Taylor-expanding Eq.[45] one obtains,

$$\begin{aligned} \overline{\nu}_2 &= \nu_2 + \frac{\gamma}{3} \\ \overline{\nu}_3 &= \frac{1}{4}(-2\gamma + \gamma^2 + 6\gamma\nu_2 + 4\nu_3) \\ \overline{\nu}_4 &= \frac{1}{27}(36\gamma - 36\gamma^2 + 8\gamma^3 - 108\gamma\nu_2 + 72\gamma^2\nu_2 + \\ &\quad + 54\gamma\nu_2^2 + 72\gamma\nu_3 + 27\nu_4), \end{aligned} \quad (47)$$

and so on.

For an arbitrary power spectrum  $P(k)$ , the above results can be trivially generalized using Eq.[44]. The results are given in Eq.[A4] of the Appendix A.

In Appendix C we present an alternative derivation of the (top-hat) smoothing effects within the SC approximation, following the kernels in Fourier space. There, one can explicitly see how in the SC model, smoothing is a trivial operation which only changes the  $\nu_n$  coefficients but not the local nature of the transformation from the linear to the non-linear density field.

## 5 COMPARISON OF THE SC MODEL WITH EXACT PT AND N-BODY SIMULATIONS

In this section we start from the exact solution to the SC dynamics in an Einstein-de Sitter universe assuming the *rms* fluctuation  $\sigma_l \lesssim 1$ . In that perturbative limit, we carry out the calculation of the connected moments for the density. Results for the velocity field are provided in Paper III.

We compare the SC predictions with those derived from the exact PT in the context of the diagrammatic approach. Although we know that the SC dynamics exactly reproduces the leading-order contribution to the cumulants, higher order effects will in general be different. We have seen that the difference is due to neglecting the shear and can therefore be attributed to non-local effects, which we will also call *tidal* effects. Note that in our context *local* refers only to the density.

As commented above, the results are derived in general for the smoothed fields for a top-hat window function, the unsmoothed fields being recovered just as the particular case  $\gamma = 0$ . To simplify the expressions, we will assume that higher order derivatives of the variance (see Appendix A, Eq.[A4] with  $\gamma_p \simeq 0$  for  $p > 2$ ) can be neglected. This is a good approximation for slowly varying  $P(k)$ , like CDM (see Scoccimarro 1998) or the APM model, but it is straightforward to take those higher order derivatives into account anyway. We do take into account  $\gamma_2$ , which for loop corrections could contribute up to 10% on small scales.

We will also compare the SC results with different N-body simulations, with parameters given in Table 1. Also given is the reference where the details for a particular run can be found. For each simulation, the cumulants  $\bar{\xi}_J$  are estimated from counts in spherical cells, as described in BGE95, where more details about the estimation are given. For the later outputs the correlations are corrected from the Poisson shot-noise (*e.g.*, BGE95). We also apply the corrections due to the ZA transient (see Baugh *et al.* 1995) as analytically derived by Scoccimarro (1998).

Following the steps described in section §4.2, we can derive now the smoothed one-point cumulants to an arbitrary perturbative order for the SC dynamics. In this case we start from Gaussian initial conditions and use the local transformation for the local smoothed density (see Eq.[46]) with  $c_k = \bar{\nu}_k$ , as given in Eq.[47], to find the leading-order and higher-order corrections for the variance and the hierarchical amplitudes. In order to handle the perturbative expansions in the cumulants for both GIC or NGIC in a general framework, we shall introduce the following notation,

$$\sigma^2 = \langle \delta^2 \rangle = \sum_i s_{2,i} \sigma_i^2 \quad (48)$$

where  $s_{2,1} \equiv 1$  and the subscript  $i$  in the coefficients label the perturbative order. For GIC the odd terms in the perturbative expansion vanish and the get for the variance,

$$\sigma^2 \equiv \sigma_G^2 = \sigma_1^2 + s_{2,4} \sigma_4^2 + s_{2,6} \sigma_6^2 + \dots \quad (49)$$

Note that our notation for GIC is equivalent to that of SF96a provided one identifies  $s_{2,2i+2} \equiv s^{(i)}$  with  $i = 1, 2, \dots$ .

On the other hand, for the hierarchical amplitudes we keep the above introduced notation with the added labeling of the order of the moment  $J$ , that defines the  $S_J$  coefficients,

$$S_J \equiv \frac{\bar{\xi}_J}{\bar{\xi}_2^{J-1}} \equiv \frac{\langle \delta^J \rangle_c}{\langle \delta^2 \rangle^{J-1}} = \sum_i S_{J,i} \sigma_i^2 \quad (50)$$

which for GIC has non-vanishing contributions from the even terms alone,

$$S_J^G = S_{J,0} + S_{J,2} \sigma_2^2 + S_{J,4} \sigma_4^2 + \dots \quad (51)$$

with  $S_{J,2i} \equiv S_J^{(i)}$  (with  $i = 0, 1, 2, \dots$ ) in SF96a notation.

As mentioned before, it is usual to denote *tree-level* to the leading order contributions,  $S_J^{(0)}$ . Although this is true for GIC, in general the leading order contributions do not correspond to the tree-level in the diagrammatic approach (see Paper II). However, for the sake of clarity, we shall maintain the notation  $S_J^{(0)}$  (or  $T_J^{(0)}$  for the velocity field, see Paper III) to denote the leading-order contribution.

With this notation the results for GIC (in terms of the SC coefficients  $\nu_k$ ) are given in Appendix A, Eq.[A2], with  $c_k = \nu_k$ . In terms of the smoothing index  $\gamma = -(n+3)$ , we have, for a power-law power spectrum  $P(k) \sim k^n$ , and a top-hat window:

$$\begin{aligned} s_{2,4} &= \frac{1909}{1323} + \frac{143}{126} \gamma + \frac{11}{36} \gamma^2 \\ s_{2,6} &= \frac{344439415}{107270163} + \frac{21651395}{3667356} \gamma + \frac{408721}{95256} \gamma^2 + \\ &+ \frac{1651}{1134} \gamma^3 + \frac{127}{648} \gamma^4 \\ S_{3,0} &\equiv S_3^{(0)} = \frac{34}{7} + \gamma \end{aligned}$$

$$\begin{aligned} S_{3,2} &= \frac{1026488}{101871} + \frac{12862}{1323} \gamma + \frac{407}{126} \gamma^2 + \frac{10}{27} \gamma^3 \\ S_{3,4} &= \frac{251978977148}{5256237987} + \frac{71492200235}{750891141} \gamma + \frac{138567091}{1833678} \gamma^2 \\ &+ \frac{79295}{2646} \gamma^3 + \frac{2891}{486} \gamma^4 + \frac{1841}{3888} \gamma^5 \\ S_{4,0} &\equiv S_4^{(0)} = \frac{60712}{1323} + \frac{62}{3} \gamma + \frac{7}{3} \gamma^2 \\ S_{4,2} &= \frac{22336534498}{83432349} + \frac{42649448}{130977} \gamma + \frac{3571621}{23814} \gamma^2 \\ &+ \frac{35047}{1134} \gamma^3 + \frac{1549}{648} \gamma^4 \\ S_{4,4} &= \frac{126152927186426522}{61923739724847} + \frac{69638296109567}{15768713961} \gamma \\ &+ \frac{8977285860007}{2252673423} \gamma^2 + \frac{7018518515}{3667356} \gamma^3 \\ &+ \frac{24548155}{47628} \gamma^4 + \frac{668971}{9072} \gamma^5 + \frac{102005}{23328} \gamma^6 \\ S_{5,0} &\equiv S_5^{(0)} = \frac{200575880}{305613} + \frac{1847200}{3969} \gamma + \frac{6940}{63} \gamma^2 + \frac{235}{27} \gamma^3 \\ S_{5,2} &= \frac{38066642685488}{5256237987} + \frac{8041429493780}{750891141} \gamma + \frac{5828197535}{916839} \gamma^2 \\ &+ \frac{45012655}{23814} \gamma^3 + \frac{955895}{3402} \gamma^4 + \frac{4052}{243} \gamma^5 \\ S_{6,0} &\equiv S_6^{(0)} = \frac{351903409720}{27810783} + \frac{3769596070}{305613} \gamma + \frac{17907475}{3969} \gamma^2 \\ &+ \frac{138730}{189} \gamma^3 + \frac{1210}{27} \gamma^4 \\ S_{6,2} &= \frac{93347762463213320}{421249930101} + \frac{2034255356621746}{5256237987} \gamma \\ &+ \frac{211757079765188}{750891141} \gamma^2 + \frac{301575001360}{2750517} \gamma^3 \\ &+ \frac{69888305}{2916} \gamma^4 + \frac{1582214}{567} \gamma^5 + \frac{14591}{108} \gamma^6 \end{aligned} \quad (52)$$

In table 2 we display a summary of results for the SC model for different values of the spectral index. Note, to start with, that for large  $n$  or more negative  $\gamma$  the coefficients decrease with the perturbative order (the subscript after the coma), indicating possible convergence of the perturbative series. For  $\gamma = 0$  (*i.e.*,  $n = -3$ ) the coefficients of each order in the expansion increases quickly with the order, which might indicate that the PT expansion does not converge for the unsmoothed field, at least in the SC approximation.

For  $S_J$ , there is a suppression of non-linearities with the effects of smoothing (as  $n$  increases from  $-3$  to  $0$ ), which is also found in numerical simulations (see *e.g.*, Lokas *et al.* 1995)). In particular, vanishing non-linearities are found for  $n \approx 0$ .

## 5.1 Comparison with Exact PT

The tree-level results in the SC model are of course identical to the ones estimated in the exact PT by Juskiwicz *et al.* (1993) and B94b, as argued in §2.2. For the *unsmoothed* fields, analytic results including the first corrective term to the tree-level, were first derived by SF96a through loop calculations in the diagrammatic approach to the exact PT. For the variance, skewness, and the kurtosis (the last one only at tree-level) they obtain,

$$\begin{aligned} \sigma^2 &\approx \sigma_1^2 + 1.82 \sigma_4^2 + \mathcal{O}(\sigma_1^6) \\ S_3 &\approx 4.86 + 9.80 \sigma_1^2 + \mathcal{O}(\sigma_1^4) \end{aligned}$$

**Table 1.** Simulation parameters

| run names      | $P(k)$             | $\Omega$ - $\Lambda$               | number<br>of particles | mesh    | $L_{box}$<br>( $h^{-1}\text{Mpc}$ ) | Reference              |
|----------------|--------------------|------------------------------------|------------------------|---------|-------------------------------------|------------------------|
| SCDM (a)-(j)   | $\Gamma = 0.5$ CDM | $\Omega = 1 \quad \Lambda = 0$     | $126^3$                | $128^3$ | 378                                 | Gaztañaga & Baugh 1995 |
| LCDM (a)-(j)   | $\Gamma = 0.2$ CDM | $\Omega = 0.2 \quad \Lambda = 0.8$ | $126^3$                | $128^3$ | 378                                 | Gaztañaga & Baugh 1995 |
| APMPK1 (a)-(e) | APM                | $\Omega = 1 \quad \Lambda = 0$     | $126^3$                | $128^3$ | 400                                 | Gaztañaga & Baugh 1997 |
| APMPK2 (a)-(b) | APM                | $\Omega = 1 \quad \Lambda = 0$     | $200^3$                | $128^3$ | 600                                 | Baugh & Gaztañaga 1996 |

| SC        | Unsmoothed   |               | Smoothed      |               |
|-----------|--------------|---------------|---------------|---------------|
|           | $\gamma = 0$ | $\gamma = -1$ | $\gamma = -2$ | $\gamma = -3$ |
|           | $n = -3$     | $n = -2$      | $n = -1$      | $n = 0$       |
| $s_{2,4}$ | 1.44         | 0.61          | 0.40          | 0.79          |
| $s_{2,6}$ | 3.21         | 0.34          | 0.05          | 0.68          |
| $S_{3,0}$ | 4.86         | 3.86          | 2.86          | 1.86          |
| $S_{3,2}$ | 10.08        | 3.21          | 0.59          | -0.02         |
| $S_{3,4}$ | 47.94        | 3.80          | 0.07          | 0.06          |
| $S_{4,0}$ | 45.89        | 27.56         | 13.89         | 4.89          |
| $S_{4,2}$ | 267.72       | 63.56         | 7.39          | -0.16         |
| $S_{4,4}$ | 2037.2       | 138.43        | 1.99          | 0.31          |
| $S_{5,0}$ | 656.31       | 292.35        | 96.50         | 16.52         |
| $S_{5,2}$ | 7242.2       | 1263.97       | 91.85         | -1.16         |
| $S_{5,4}$ | 80903.0      | 4363.92       | 42.89         | 1.53          |
| $S_{6,0}$ | 12653.49     | 4141.58       | 876.62        | 67.81         |
| $S_{6,2}$ | 221597.1     | 28256.19      | 1274.38       | -8.04         |
| $S_{6,4}$ | 3405857.8    | 140641.3      | 906.74        | 7.88          |

**Table 2.** Values for the higher-order perturbative contributions in the SC model for the unsmoothed ( $n = -3$ ) and smoothed ( $n = -2, -1, 0$ ) density fields, for a top-hat filter and a power-law power spectrum.

$$S_4 \approx 45.89 + \mathcal{O}(\sigma_i^2), \quad (53)$$

for the average values in the range  $2 \geq n \geq -2$  (for a power-law power spectrum,  $P(K) \sim k^n$ ), with a 3% variation within that range due to non-local effects. The above results are to be compared to those from the SC in the perturbative regime (truncated at the same order),

$$\begin{aligned} \sigma^2 &\approx \sigma_i^2 + 1.44 \sigma_i^4 + \mathcal{O}(\sigma_i^6) \\ S_3 &\approx 4.86 + 10.08 \sigma_i^2 + \mathcal{O}(\sigma_i^4) \\ S_4 &\approx 45.89 + 267.72 \sigma_i^2 + \mathcal{O}(\sigma_i^4). \end{aligned} \quad (54)$$

Comparing with the exact PT result Eq.[53], we can see that tidal (non-local) effects only amount to a 3% in the

corrective term for  $S_3$  and up to 20% in the first corrective term for the variance. The  $S_4$  correction ( $\sim 268 \sigma_i^2$ ) must be taken as an accurate prediction for  $S_4$  (within the few per cent effect expected from the net tidal contribution for the  $S_J$  ratios) since there are no analytic results available to compare with. We therefore see from the above comparison that the shearless (SC) approximation leads to very accurate predictions for the hierarchical amplitudes,  $S_J$ , while giving worse estimates for the cumulants,  $\xi_J$ .

We stress the importance of applying the SC approximation in Lagrangian space, where is the exact spherically symmetric solutions of the field equations. The SC model is described by a transformation that *only* depends on the value of the linear field at the same point (what we call a *local-density transformation*). When going back to Euler space the density fluctuation (defined at a point) is normalized with a factor (see Eq.[39]) which is a function of the (non-linear) variance. Since the variance is a volume average of the two-point correlation function, this factor yields some *non-local* contribution to the cumulants (in Euler space). This *non-local* contribution is missed when introducing the SC model in Euler space *directly*, thus is not surprising that the predictions for the cumulants in the SC approximation in Euler space are a poor estimation of those in exact PT, as the latter are dominated by the non-local (tidal) effects (see Table B in Appendix B). The contribution to the cumulants of this *non-local* term is typically negative so the predictions from the SC model in Euler space generically overestimate those in Lagrangian space. However, the domination of non-local effects in the cumulants for the SC model in Euler space is partially canceled when computing the hierarchical ratios  $S_J$ , similarly to what is found for the SC model in Lagrangian space. We shall see below that *smoothing* effects do not alter substantially this interpretation (at least for a top-hat window).

For the *smoothed* fields, there are few analytic results which concentrate on the variance (and its Fourier transform, the power-spectrum), the skewness, and the bispectrum. For the present analysis we focus on the results for the variance and the skewness (see SF96b and Scoccimarro 1997, hereafter S97, respectively) which, in the diagrammatic approach to the exact PT to one-loop order, for a top-hat smoothing and  $n = -2$ , give

$$\begin{aligned} \sigma^2 &\approx \sigma_i^2 + 0.88 \sigma_i^4 + \mathcal{O}(\sigma_i^6) \\ S_3 &\approx 3.86 + 3.18 \sigma_i^2 + \mathcal{O}(\sigma_i^4) \end{aligned} \quad (55)$$

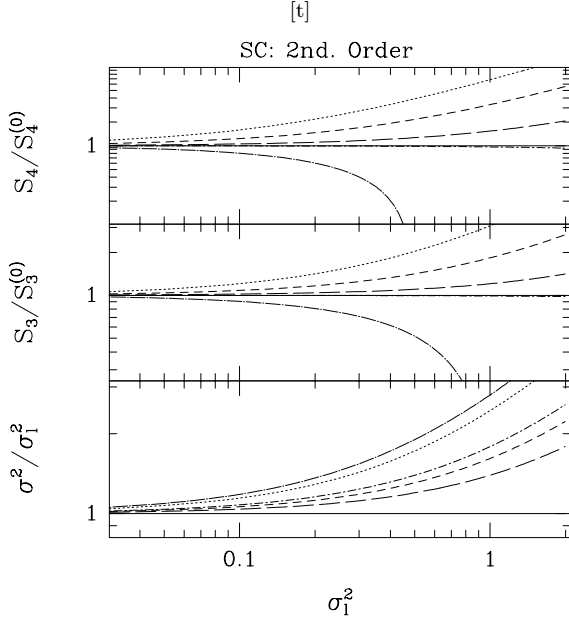


**Figure 1.** Departures from the tree-level contributions as the linear *rms* fluctuation grows, for the variance, skewness and kurtosis of the density field as predicted by the SC model up to the 2nd non-vanishing perturbative contribution (one-loop) for different values of the spectral index: the dotted line shows the  $n = -3$  (unsmoothed) case, and the short-dashed ( $n = -2$ ), long-dashed ( $n = -1$ ), dot short-dashed ( $n = 0$ ), dot long-dashed ( $n = 1$ ) depict the behavior for the smoothed density field. The solid line shows the tree-level values as a reference. The corrective term has a minimum contribution to the variance for  $n \approx -1$ , while the hierarchical amplitudes show a vanishing one-loop contribution for  $n \approx 0$ .

that we compare to the SC predictions,

$$\begin{aligned} \sigma^2 &\approx \sigma_l^2 + 0.61 \sigma_l^4 + \mathcal{O}(\sigma_l^6) \\ S_3 &\approx 3.86 + 3.21 \sigma_l^2 + \mathcal{O}(\sigma_l^4) \end{aligned} \quad (56)$$

which means a 30% and 1% contribution from the tidal forces for the corrections in the variance and the skewness, respectively. These can be obtained by just subtracting the shearless (SC) contribution to the exact computation carried out by means of the loop calculations. Thus, we see that in line with the unsmoothed predictions, the shearless contribution completely dominates the skewness  $S_3$ , at least at the one loop order.

In Fig 1 we display the departures from the tree-level contribution for the evolved variance when the one-loop correction is included, skewness and kurtosis as the linear variance approaches unity, where the perturbative regime is expected to break down. Fig 2 shows the same as Fig 1 when the 3rd order (3rd non-vanishing contribution) is included in the computation of the cumulants: the qualitative features are preserved when this higher-order contribution is taken into account with respect to those inferred from the 2nd order analysis. Only a monotonic enhancement of the scaling properties is observed.

In Table 3 we compare the results from different approximations to the exact dynamics in the perturbative regime (exact PT), available in the literature and we give as well the SC predictions in the same regime. We recall that the FFA

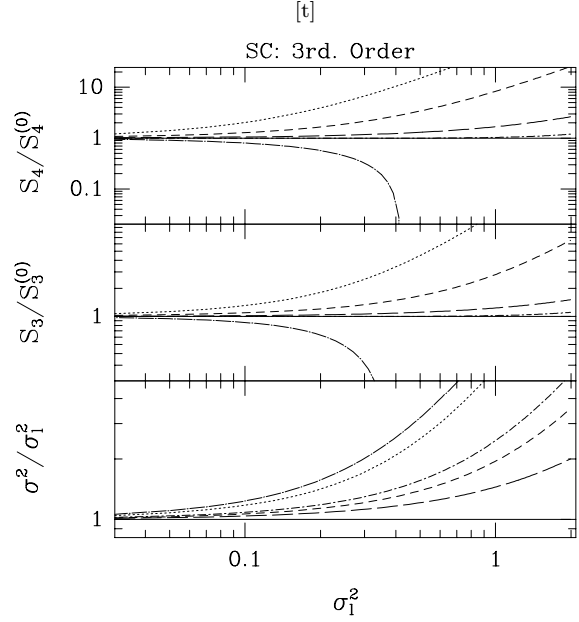


**Figure 2.** Same as Fig 1 when the 3rd perturbative contribution (two-loop) is included in the computation of the cumulants.

| Dynamics         | $s_{2,4}$ | $S_{3,0}$ | $S_{3,2}$ | $S_{4,0}$ | $S_{4,2}$ |
|------------------|-----------|-----------|-----------|-----------|-----------|
| <i>FFA*</i>      | 0.43      | 3         | 1         | 16        | 15.0      |
| <i>LPA*</i>      | 0.72      | 3.40      | 2.12      | 21.22     | 37.12     |
| <i>ZA*</i>       | 1.27      | 4         | 4.69      | 30.22     | 98.51     |
| <i>SC</i>        | 1.44      | 4.86      | 10.08     | 45.89     | 267.72    |
| <i>Exact PT*</i> | 1.82      | 4.86      | 9.80      | 45.89     | ?         |

**Table 3.** Comparison between different non-linear approximations to the for the *unsmoothed* fields up to the first corrective term beyond tree-level (the *one-loop* term). The asterisk denotes the results obtained within the diagrammatic approach for the relevant dynamics.

is based on a linearization of the peculiar velocity field. The LPA assumes the potential remains linear throughout the gravitational evolution, and the ZA takes the trajectories of the particles to be straight lines. All values concerning the one-loop contribution (including the exact PT ones), except for the SC ones, are derived making use of the diagrammatic formalism and are given in SF96a. Tree-level amplitudes had been derived previously though and a summary of those results may be found in Bernardeau *et al.* (1994). As summarized in Table 3, the SC model yields the best estimates for the loop corrections in PT within the available non-linear approximations.

## 5.2 Previrialization in the Variance

It is important to notice the different behavior between the cumulants (like the variance) and the hierarchical amplitudes,  $S_J$ . It has long been argued that non-local evolution-

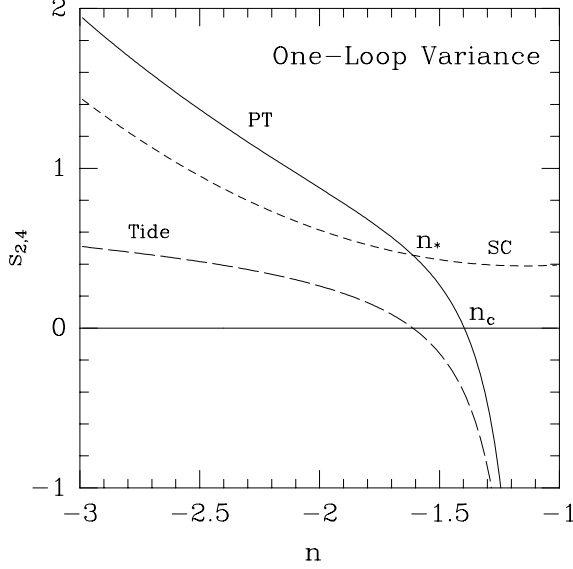


**Figure 3.** The one-loop contribution to the variance in PT. The solid line depicts the exact PT behavior, the short-dashed line shows the shearless (SC) contribution while the long-dashed line gives the tidal contribution. Two characteristic indices arise in this analysis:  $n_c \simeq -1.4$  where the one-loop variance vanishes, and  $n_* \simeq -1.6$ , where tidal effects are zero and the SC model prediction is exact.

any effects generate a suppression of collapse on the largest scales due to the increase in small-scale power that generates large scale random motions, the so-called effect of *previrialization* (see Davis and Peebles 1977, Peebles 1990, Lokas *et al.* 1996). This will result in a non-linear variance that is smaller than the linear one within a certain range. This effect has been found in N-body simulations (*e.g.*, see Figure 9 in BGE95).

The local picture arising from the SC model is unable to account for a complete suppression of non-linearities in the large scale density (and velocity) fields and yields a faster growth of fluctuations on the large scales compared to the actual non-local dynamics. This qualitative feature of the SC model was already pointed out by Bernardeau (1994c), in what he called the *rare event limit*,  $\delta_l/\sigma_l \rightarrow \infty$ . Making use of the third order in PT (in Lagrangian space) for the density field *smoothed* with a top-hat window (see his Eq.[38]) for a scale free power spectrum, he claimed that the SC picture deviates from the exact PT as smoothing effects increase. In particular, he found that for a spectral index  $n \gtrsim -1$ , PT diverges due to the shear effects. Whenever more realistic spectra (models with a cut-off on small scales, such as CDM or APM-like ones) are introduced, this divergence becomes only logarithmic.

In PT, the above commented suppression depends on the smoothing effects and leads to the appearance of a critical value of the spectral index (assuming scale free power spectrum) around  $n_c \approx -1.4$  (see S97), for which non-linear contributions vanish. Figs 1 and 2 illustrate well this point since no change of sign in the first non-linear contribution (beyond tree-level) to the evolved variance is appreciated in the plot contrary to what has been found in numerical sim-

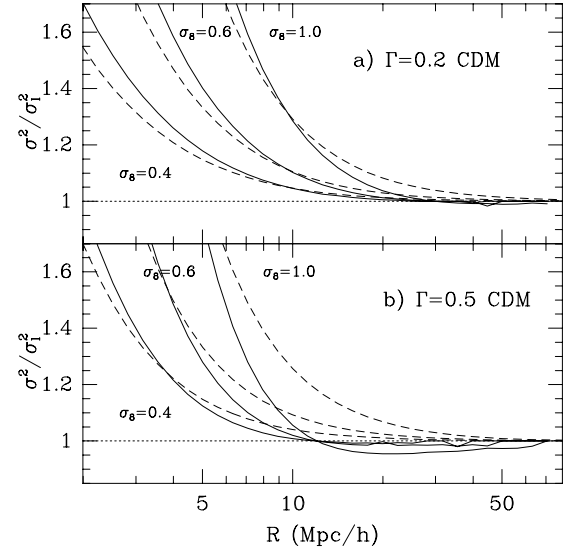


**Figure 4.** The variance in spherical shells of radius  $R$ . We compare linear theory to the SC model and the exact PT (leading order) non-linear correction, against the linear term. Each panels, (a) and (b), show the ratio of the non-linear to the linear variance for the  $\Gamma = 0.2$  (a) or  $\Gamma = 0.5$  (b) CDM initial  $P(k)$ . In both cases the continuous line from bottom to top corresponds to  $\sigma_8 = 0.4, 0.6, 1.0$ . The SC predictions for the same amplitudes are shown as dashed lines.

ulations depicting the exact perturbative scaling (see Lokas *et al.* 1996, Fig 4). Note that the SC prediction yields a minimum contribution at  $n \simeq -1.14$ , which is not far from  $n_c \approx -1.4$ , but the net effect at the minimum is non-zero.

Comparing the results for the variance from the exact PT and the shearless (SC) approximation, we can infer some information about where the tidal effects become lower, comparable or greater than the shearless contribution, provided the variance changes smoothly. Let us formally decompose the one-loop contribution to the variance in the shearless (SC) and tidal contributions as follows,

$$s_{2,4}^{PT} = s_{2,4}^{SC} + s_{2,4}^{Tide}, \quad (57)$$

where  $s_{2,4}^{SC} > 0$  for all  $n$  as displayed on the bottom panel of Fig 1. The one-loop contribution to the variance in PT,  $s_{2,4}^{PT}$  can be integrated from the analytic expression for the one-loop power-law power spectrum given in SF96b (see their Eq.[B5]) valid in the range  $-1 > n > -3$ . As shown in Fig. 3, the shearless (SC) contribution gives a systematic underestimation of the PT value from the unsmoothed value ( $n = -3$ ) up to  $n_* \simeq -1.6$  where the tidal contribution vanishes, and thus,  $s_{2,4}^{PT} = s_{2,4}^{SC}$ . Around this index, the SC model gives an accurate estimation of the one-loop variance. Beyond this point,  $n \gtrsim n_*$ , the tidal contribution rapidly grows and becomes negative (see Fig.3). For  $n_c \simeq -1.4$ ,  $s_{2,4}^{SC} = -s_{2,4}^{Tide}$  and the one-loop variance vanishes. As seen in the plot, while the shearless contribution remains positive and small, the tidal contribution takes larger and larger negative values as  $n \rightarrow -1$ , what breaks down the PT approach (at least for the variance).

In Figure 4 we compare the non-linear evolution of the variance for the SC to that of the exact PT. We present

the ratio of the non-linear to the linear variance from CDM model, with  $\Gamma = 0.2$  (top panel) and  $\Gamma = 0.5$  (bottom), as a function of the smoothing radius. The leading order non-linear SC predictions are shown as dashed lines. The corresponding (numerically integrated) PT results are shown as continuous lines. These are estimated from  $P(k)$  to second order (2nd non-vanishing contribution) as obtained following Baugh & Efstathiou (1994). In both cases we show results for different amplitudes of the linear variance:  $\sigma_8 = 0.4, 0.6, 1.0$ , which has a linear variance  $\sigma \simeq 0.5$  at scales  $R \simeq 6, 10, 15 h^{-1}$  Mpc, respectively. We can define an *effective index*,  $n_{eff}$ , as the index at the scale where the variance becomes unity. For the  $\Gamma = 0.2$  model we have that  $n_{eff}^{\Gamma=0.2} \simeq -2$ , while for  $\Gamma = 0.5$  this is about 0.5 larger (this can be seen for example in Figure 9 in Croft & Gaztañaga 1998):  $n_{eff}^{\Gamma=0.5} \simeq -1.5$ . The SC prediction should match better the  $\Gamma = 0.2$  model, as the effective index is closer to  $n_*$ , where tidal effects vanish. For the  $\Gamma = 0.5$  model we have that  $n_{eff} \simeq n_c$  and the SC model is not such a good approximation. In this case we expect non-linear effects to be small due to the cancellation of tidal and purely local contributions to the cumulants. This can be seen in Figure 4. The SC model matches well the PT prediction for the  $\Gamma = 0.2$  model, where non-linear effects are more important. It also matches well the earlier evolution of  $\Gamma = 0.5$  model, for small amplitudes of  $\sigma_l$ , *e.g.*, earlier outputs given by smaller  $\sigma_8$ . For the later outputs (*e.g.*,  $\sigma_8 = 1$  in Figure 4, bottom panel) tidal effects become important canceling out the non-linear growth (previrialization effect). This is not fully recovered by the SC model (which only accounts for the local effects). Nevertheless note that for small scales, where the variance is large, the prediction seems to be dominated by the local effects and the SC model also recovers the exact prediction.

In Figure 5 we show the non-linear evolution of the variance as the ratio to the linear variance from CDM N-body simulations with  $\Gamma = 0.5$  (filled triangles) and  $\Gamma = 0.2$  (open triangles) as a function of the smoothing radius. The error-bars, from 10 realizations of the models, which are not displayed for clarity, are always smaller than the symbols except for the last 3 points where the error-bars are smaller than twice the size of the symbols. In both cases  $\sigma_8 = 0.5$  and the linear variance  $\sigma \simeq 1$  at  $R \simeq 2 h^{-1}$  Mpc. The SC predictions are shown as dashed lines, which are to be compared to the exact PT results (continuous lines). For the  $\Gamma = 0.2$  model there is hardly any difference between the predictions and the N-body results. In fact, the latter follows both predictions up to large values of  $\sigma$  (small scales). For the  $\Gamma = 0.5$  model, non-linear effects are small during the weakly non-linear phase and both linear and non-linear predictions are close to the N-body results. There is a slight sign of previrialization at  $R \simeq 20 h^{-1}$  Mpc, but the effect is quite small. This way, despite the exact PT results are more accurate in qualitative terms, there is little difference in practice. Note that, in this case, the agreement with predictions does not extend to large values of  $\sigma$  (small scales) unlike the case of the  $\Gamma = 0.2$  model.

Figure 6 shows the corresponding results for  $\sigma_8 = 1$ . In this case, the  $\Gamma = 0.2$  CDM model is the one with an effective index  $n_{eff} \simeq n_c$  so that non-linear effects are small and we have a similar situation to the  $\Gamma = 0.5$  model at  $\sigma_8 = 0.5$ . The effective index for  $\Gamma = 0.5$  model at  $\sigma_8 = 1.0$

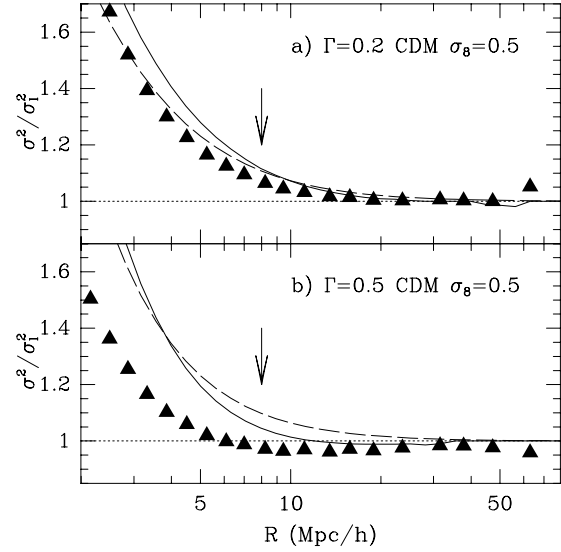


**Figure 5.** Non-linear evolution of the variance. Symbols show the ratio of the non-linear to the linear variance from CDM N-body simulations with  $\Gamma = 0.2$  (top panel) and  $\Gamma = 0.5$  (bottom panel) as a function of the smoothing radius. In both cases  $\sigma_8 = 0.5$ . The SC model predictions are shown as a short-dashed line while PT predictions are shown as a continuous line. The arrows indicate where  $\sigma_l = 0.5$ .

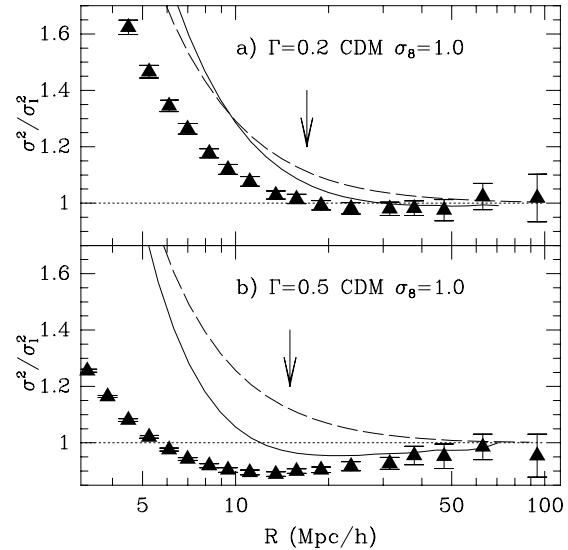


**Figure 6.** Same as Fig. 5 for  $\sigma_8 = 1.0$ .

si  $n > n_c$  so that the previrialization effect discussed above is larger and the SC prediction fails (long-dashed line). The prediction for the second order contribution to  $P(k)$  for  $\Gamma = 0.5$  is shown as a continuous line. Although it shows some previrialization effect (the ratio is smaller than unity), it only fits the N-body results in the narrow range of scales,  $R \gtrsim 30 h^{-1}$  Mpc, where linear theory is a good approximation, given the errors. The above arguments explain in a sim-

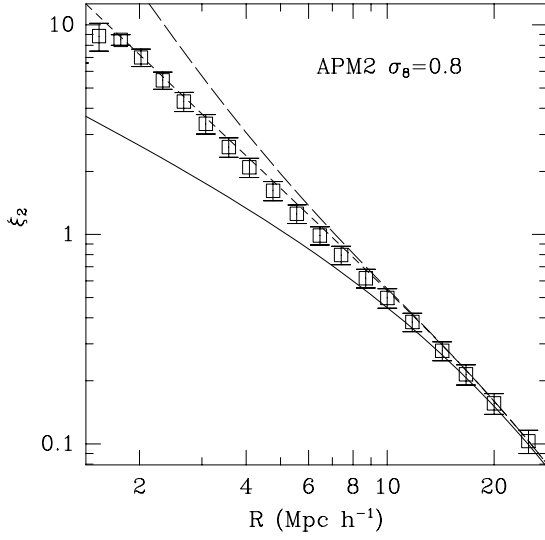


**Figure 7.** The variance for APM2 at  $\sigma_8 = 0.8$  (figures) compared to PT models (lines): (a) linear theory prediction (continuous line), (b) the 2nd order result, *i.e.*, when the 2nd perturbative contribution to the variance is included in the SC (short dashed lines) (c) the 3d order result in the SC (long dashed lines).

ple fashion why the SC model matches so well the variance of the APM simulations even on small scales (for output times  $\sigma_8 \lesssim 1$ ) as shown in Fig. 7. The effective index  $n_{eff}$  on the quasi-linear scales is within the range  $-2 \gtrsim n_{eff} \gtrsim -1.5$ , a bit lower than the  $\Gamma = 0.2$  CDM model (see Fig.3 in BG96, where quasi-linear scales correspond to  $k \simeq 0.1$ ). For this index, tidal effects are expected to give a sub-dominant contribution. Although the SC model seems to match well the simulations up to the scales where the linear variance  $\sigma_l \gtrsim 1$ , *e.g.*, beyond the point where PT must break down, the third order SC correction (long-dashed line) shows significant deviations already at  $R \simeq 6 h^{-1}$  Mpc, where  $\sigma_l \simeq 1$ .

The results here obtained are in qualitative agreement with those found by B94c, according to which, the *rare event limit* progressively differs from the exact PT predictions as  $n \rightarrow -1$ , even in the first correction to the variance  $s_{2,4}$ . Furthermore, B94c also finds no indication of *previrialization* in the *rare event limit* and stresses the unimportance of this effect for the APM & IRAS observations, given the effective spectral index related to the scales on which they lie ( $n_{eff} \simeq -1.3, -1.4$ , respectively). However, according to B94c, the *rare event limit* is *always* different from the exact PT result whenever  $\delta_l \neq 0$ . This is at variance with what we find here, where the SC model is expected to yield accurate results, particularly for values of the spectral index  $n \in [-1.5, -2]$ . What is more, there must be some value  $n_*$  within that interval for which tidal effects exactly vanish.

### 5.3 Comparison of the $S_J$ Ratios with N-body Simulations: Previrialization Lost

On the other hand, when it comes to evaluating the hierarchical amplitudes,  $S_J$ , it turns out that the cancellation of (non-local) tidal effects erases the previrialization effect

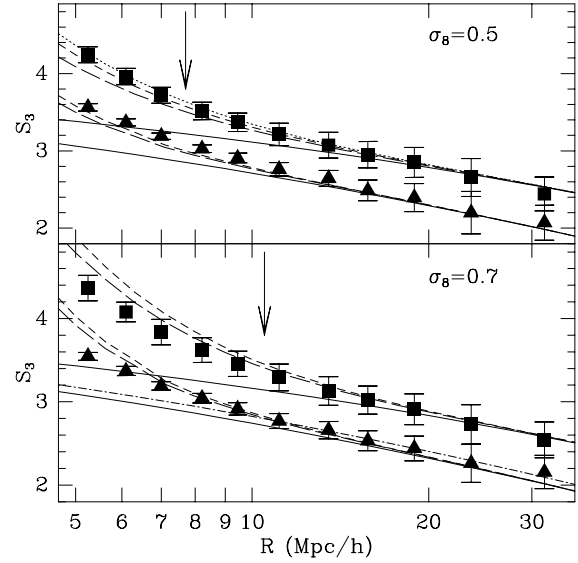


**Figure 8.** The hierarchical skewness  $S_3$  from 10 realizations of flat CDM N-body simulations at output time  $\sigma_8 = 0.5$  (top panel) and  $\sigma_8 = 0.7$  (bottom panel). Symbols with error-bars correspond to  $\Gamma = 0.2$  (squares), and  $\Gamma = 0.5$  (triangles). Each case is compared to the corresponding PT predictions (lines): a) the PT tree-level prediction uncorrected for the ZA transients (dot-dashed line), and corrected for the transients (continuous), b) the 2nd order result in the SC uncorrected for the ZA transients (short-dashed), corrected for the ZA transients (long-dashed), and the case with  $\gamma_2 = 0$  (dotted). The arrows show where  $\sigma = 0.5$ . The dot-dashed line shows the tree-level prediction for the  $\Gamma = 0.5$  and  $\sigma_8 = 0.7$ , uncorrected for the ZA transient.

and the suppression of non-linearities at the first corrective order beyond tree-level appears at a different spectral index  $n \approx 0$ , what seems to be an intrinsic (local) shearless feature if the good agreement between the local (SC) and non-local (exact PT) hierarchical amplitudes is anything to go by. Furthermore, loop-calculations in Fourier space concerning the reduced Bispectrum,  $Q$ , seem to confirm this argument as the scale dependence of  $Q$  retains non-vanishing non-linearities even at  $n \approx -1.5$  (at least for the equilateral configuration, see Scoccimarro *et al.* 1998, Eq.[30]). However, the reduced bispectrum also preserves some non-local features which manifest in terms of a loss of configuration dependence (isotropization) roughly at the same value of the spectral index as the one estimated from the variance or the power spectrum,  $n_c \approx -1.4$  (see SF96b, and S97).

In Figs 8, we compare the SC predictions with CDM simulations for two different models. The smoothing coefficients  $\overline{\nu}_k$  are modified to include the higher-order logarithmic derivatives of the variance (see Eq. [A3] in Appendix A) but it turns out that, within the errors, they do not significantly change the predictions derived from the power-law power spectrum. At small scales  $\gamma_2$  changes  $S_3$  by less than 10%, which hardly makes any difference given the errors, as shown by the dotted line, only displayed for the  $\Gamma = 0.2$   $\sigma_8 = 0.05$  model for clarity. The error bars shown in the SCDM plot are derived from 10 realizations. The arrows in the Figure show the scale at which  $\sigma = 0.5$ .

On large scales the spectral index  $n$  for CDM models

becomes larger and non-linearities are very small, as predicted by the SC model (see Table 2). This explains why deviations from the tree-level are hardly noticeable in the later outputs (bottom panel) and they only become important, given the errors, when PT theory should break down ( $\sigma_l \simeq 1$ ). The effective index in the earlier outputs is smaller (corresponding to smaller scales) and deviations from tree-level are more significant. In this regime the SC predictions show a very good agreement with the N-body simulations (top panel) up to  $\sigma \simeq 1$ . Note that the predictions for the exact PT corrections are not available in this case, but the agreement with the N-body simulations indicates that the SC models provides an excellent approximation.

We have corrected for ZA transients, an artifact due to the initial (ZA) start in the N-body simulations (see BGE95 1995, Scoccimarro 1998). We use the analytic results of Scoccimarro (1998) for the tree-level:

$$S_{3,0} = \frac{34}{7} + \gamma - \frac{2}{5}a^{-1} - \frac{16}{35}a^{-7/2} \quad (58)$$

where  $a$  is the expansion factor away from the (ZA) IC. In principle this is not a very important correction for the tree-level result, as the sampling errors on large scales, where  $\sigma$  is small, are large. This is more important for smaller scales, as the errors are smaller. In Figs 8 we show the tree-level prediction for  $a \rightarrow \infty$  (dot-dashed line) as compared to the actual prediction, including the transient, for  $a = 5.0$  (the bottom continuous line) in the  $\Gamma = 0.5$  model for  $\sigma_8 = 0.7$ . The long-dashed line shows the 2nd order (one-loop) prediction in the SC model corrected for the ZA transients. This can be done by using the tree-level results for the transients, as they determine all higher-orders in the SC model. As pointed out by Scoccimarro, the effects of the transients tend to create the false impression that the tree-level PT has a wider range of validity. In our case, by comparing the points to the dot-dashed line one might conclude that tree-level results are valid up to  $R \simeq 9 h^{-1}$  Mpc, while a comparison to the corrected prediction (continuous line) indicates  $R \simeq 15 h^{-1}$  Mpc. On the other hand, adding the loop terms to the uncorrected tree-level would give the false impression of a poor agreement with the SC model.

Figs 9 and 10 display the scaling of the higher-order moments according to the APM-like simulations (the mean of APMPK1 and APMPK2 in Table 1). As for the previous cases, the SC model matches well the observed behavior for the higher-orders in the N-body simulations up to the scales where PT is expected to break down, *e.g.*,  $\sigma_l \approx 1$ . As we consider higher order moments, deviations from the tree-level prediction are larger, a trend that is reproduced by the SC predictions. We have found a similar trend for higher orders in the CDM models.

The ZA transients, shown as dot-dashed lines in Fig. 9, are not very important in this case ( $a \simeq 6$ ). The effect of using  $\gamma_2 = 0$  is also small although it tends to introduce a slight shift in the predictions.

These results extend the domain of applicability of the SC model in PT beyond the point expected from B94c analysis of the *rare event limit*, as potential cancellations of the tidal contributions in the  $S_J$  ratios were not examined there.

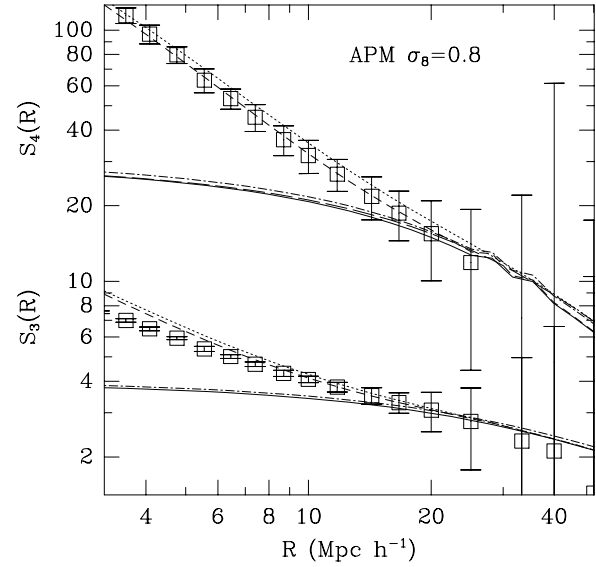


**Figure 9.** The skewness,  $S_3$ , and kurtosis,  $S_4$  for simulations of the APMPK at  $\sigma_8 = 0.8$  (open squares with error-bars) compared to tree-level theory prediction (continuous line) and the 2nd order result ( $S_J$  including the one-loop term) in the SC (short dashed lines). The corresponding predictions for  $\gamma_2 = 0$  are shown as long-dashed and dotted lines respectively. The dot-dashed lines show the tree-level predictions uncorrected for the ZA transients.

## 6 DISCUSSION AND CONCLUSIONS

No available analytic approximations to the dynamics of cosmological perturbations lead to accurate predictions for the one-point cumulants in the non-linear regime (see §3.7). This applies to all popular approximations, such as those based on putting some constraints on any of the fields that couple to the density (such as the FFA or the LPA), the Zel'dovich Approximation (ZA), which puts a constraint on the trajectories of the masses, or the local Lagrangian approximations, which assume that the evolution of the density contrast may be described locally, *i.e.*, without any influence of the surrounding matter to the mass trajectory. Despite giving some useful insight to the exact dynamical picture with much simpler calculations, none of them is able to reproduce the exact values of the one-point cumulants even at tree-level as derived in the exact PT.

As mentioned in the introduction, there are serious difficulties in applying the exact PT approach to find the gravitational evolution of the cumulants of a Gaussian field to higher-order (loop) corrections, *i.e.*, to compute next-to-leading orders. For non-Gaussian initial conditions this problem is apparent even to leading order (in non-linear corrections). An important simplification is found when only the *monopole* or spherical contribution is considered. This contribution is exact for all the tree-graphs. We have shown how the solution in this case can be found directly from the dynamical equations of the evolution of a cosmic fluctuating field (see *e.g.*, Appendix 4.3 and Appendix D) as it is given by the spherical collapse (SC) model for the case of density fluctuations for a non-relativistic pressureless ir-



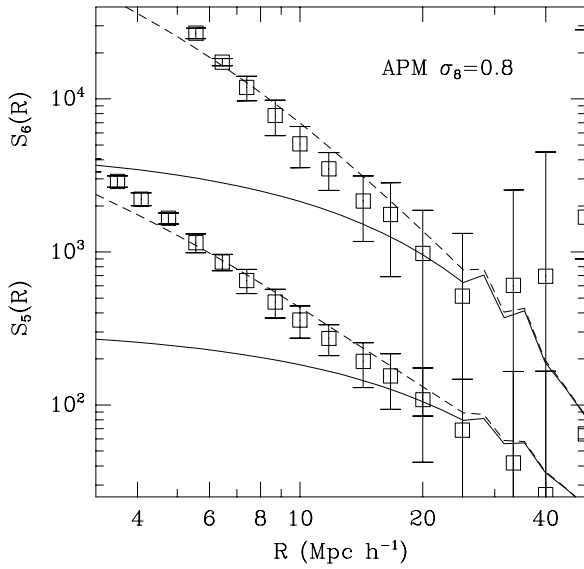


Figure 10. Same as Fig. 9 for  $S_5$  and  $S_6$ .

rotational fluid. This provides us with a simpler derivation and interpretation of the results presented by Bernardeau (1992), showing why the SC model gives the exact tree-level in PT. This lacked a satisfactory explanation in the work of Bernardeau.

We have explored the predictions for the one-point cumulants of the density field in the weakly-nonlinear regime within the *spherically symmetric* approximation to the dynamics. This is done both for the exact dynamics and for the Zel'dovich approximation (see Appendix D). As the SC model gives the exact tree-level irrespective of the nature of the initial fluctuations and the value of  $\Omega$ , it can also be used to make predictions for non-Gaussian initial conditions (the results are presented in the accompanying Paper II), the velocity field and the  $\Omega$ -dependence of these predictions (see Paper III of the series).

A natural shortcoming of the SC model is the loss of *previrialization*, i.e., the generation of large scale random motions induced by the small scale power, which is a non-local phenomenon. This is in qualitative agreement with the analysis given in B94c in the *rare event limit* to PT which is described by the SC model. The lack of *previrialization* is illustrated by the absence of vanishing non-linearities in the variance for a critical index  $n_c \approx -1.4$  (see §5.2), which is a direct consequence of *previrialization*. This phenomenon is expected from the exact PT (SF96b) and it has been observed in numerical simulations (Lokas *et al.* 1995).

Despite this, we have shown that the SC model also yields accurate predictions for the cumulants beyond the tree-level. Tidal effects in the variance are actually small because the effective index  $n_{eff}$ , as measured in galaxy catalogues (such as the APM), is  $n_{eff} \simeq [-1, -2]$  (see §5.2) for which either non-linearities are small or tidal effects are sub-dominant.

We stress the importance of applying the SC approximation in Lagrangian space. There, the SC model is de-

scribed by a transformation that *only* depends on the value of the linear field at the same point (what we call a *local-density transformation*). However, when going back to Euler space the density fluctuation (defined at a point) is normalized with a factor (see Eq.[39]) which is a function of the (non-linear) variance. Since the variance is a volume average of the two-point correlation function, this factor yields some *non-local* contribution to the cumulants (in Euler space). This *non-local* contribution is missed when introducing the SC model in Euler space *directly*, thus is not surprising that the predictions for the cumulants in the SC approximation in Euler space are a poor estimation of those in exact PT, as the latter are dominated by the non-local (tidal) effects (see Table B in Appendix B). The contribution to the cumulants of this *non-local* term is typically negative so the predictions from the SC model in Euler space generically overestimate those in Lagrangian space.

For the predictions within the SC model (in Lagrangian space) for the hierarchical ratios,  $S_J$ , tidal effects partially cancel out, at least to one-loop. We find an excellent agreement for the hierarchical amplitudes  $S_J$  in the perturbative regime of the SC model, with those derived by SF96a for the exact PT in the diagrammatic approach. A similar conclusion follows for the Zel'dovich dynamics (Appendix D), where the monopole approximation (the SSZA) results are in excellent agreement with the exact calculations.

We have also compared the predictions for the higher-order moments from the SC model to those measured in CDM and APM-like N-body simulations, and they turned out to be in very good agreement in all cases up to the scales where  $\sigma_l \approx 1$ , supporting our view that the tidal effects have only a marginal contribution to the reduced cumulants. Furthermore, the break down of the shearless approximation roughly coincides with the regime for which the perturbative approach itself breaks down,  $\sigma \simeq 0.5$ . That is, where the contribution of the second (one loop) and the third (two loop) perturbative order in the SC model are significantly different.

These results extend the domain of applicability of the SC model in PT beyond the point expected from B94c analysis of the *rare event limit*, as potential cancellations of the tidal contributions in the  $S_J$  ratios were not examined there.

Future work intended to extend the SC model should try to incorporate the local contribution to the tidal field by including other multipoles in the kernels  $F_n$ , e.g., including the shear by using the dipole contribution.

## ACKNOWLEDGMENTS

We want to thank Roman Scoccimarro, Francis Bernardeau and Josh Frieman for carefully reading the manuscript and pointing out useful remarks. EG acknowledges support from CIRIT (Generalitat de Catalunya) grant 1996BEAI300192. PF acknowledges a PhD grant supported by CSIC, DGICYT (Spain), projects PB93-0035 and PB96-0925. This work has been supported by CSIC, DGICYT (Spain), projects PB93-0035, PB96-0925, and CIRIT, grant GR94-8001.

## 7 REFERENCES

- Bagla, J.S., Padmanabhan, T., 1994, MNRAS, 266, 227  
 Bardeen, J., Bond, J.R., Kaiser, N., Szalay, A.S., 1986 ApJ, 304, 15  
 Baugh, C.M., Efstathiou, G., 1994, MNRAS, 270, 183  
 Baugh, C.M., Gaztañaga, E., Efstathiou, G., 1995, MNRAS, 274, 1049 (BGE95)  
 Bernardeau, F., 1992, ApJ, 392, 1 (B92)  
 Bernardeau, F., 1994a, A&A 291, 697 (B94a)  
 Bernardeau, F., 1994b, ApJ, 433, 1 (B94b)  
 Bernardeau, F., 1994c, ApJ, 427, 51 (B94c)  
 Bernardeau, F. & Kofman, L., 1995 ApJ, 443, 479  
 Bernardeau, F., Singh, T.P., Banerjee, B., Chitre, S.M., 1994, MNRAS, 269, 947  
 Bertschinger, E., Jain, B., 1994., ApJ, 431, 486  
 Brainerd, T., Scherrer, R.J., Villumsen J. V., 1993, ApJ, 418, 570  
 Colombi, S., Bouchet, F.R., Hernquist, L., 1996, ApJ, 465, 14  
 Croft, R.A.C., Gaztañaga, E., 1998, ApJ, 495, 554  
 Davis, M., Peebles, P.J.E., 1977, ApJS, 34, 425  
 Fosalba, P. & Gaztañaga, E., 1998, MNRAS, in press (Paper III, this issue)  
 Fry, J.N., 1984, ApJ, 279, 499  
 Fry, J.N., Gaztañaga, E., 1993, ApJ, 413, 447  
 Gaztañaga, E. & Baugh, C.M., 1995, MNRAS Lett., 273, L1  
 Gaztañaga, E. & Fosalba, P., 1998, MNRAS, in press (Paper II, this issue)  
 Goroff, M.H., Grinstein, B., Rey, S.J., Wise, M.B., 1986, ApJ, 311, 6  
 Hui, L., Bertschinger, E., 1996, ApJ, 471, 1  
 Jain, B., Bertschinger, E., 1994., ApJ, 431, 495  
 Juszkiewicz, R., Bouchet, F.R., Colombi, S., 1993 ApJ.Lett., 412, L9  
 Kaiser, N., 1984, ApJ.Lett., 284, L9  
 Kofman, L., Pogossyan, D., 1995, ApJ, 442, 30  
 Lokas, E.L., Juszkiewicz, R., Weinberg, D., Bouchet, F.R., 1995, MNRAS, 274, 730  
 Lokas, E.L., Juszkiewicz, R., Bouchet, F.R., Hivon, E., 1996, ApJ, 467, 1  
 Matarrese S., Lucchin F., Moscardini L., Saez D., 1992 MNRAS, 259, 437  
 Matsubara, T., 1994, ApJ, 434, 43  
 Mo, H.J., White, S.D.M., 1996, MNRAS, 282, 347  
 Munshi, D., Sahni, V., Starobinsky, A.A., 1995, Astron. Soc. of India Bulletin, 23, 564  
 Peebles, P.J.E., 1980, *The Large Scale Structure of the Universe*: Princeton University Press, Princeton  
 Peebles, P.J.E., 1990, ApJ, 365, 27  
 Press, W.H., Schechter, P., ApJ, 187, 425  
 Protogeris, Z.A.M., Scherrer, R.J., 1997, MNRAS, 284, 425 (PS97)  
 Scoccimarro, R., 1997, ApJ, 487, 1 (S97)  
 Scoccimarro, R., 1998, ApJ, submitted, preprint astro-ph/9711187  
 Scoccimarro, R., Frieman, J., 1996a, ApJS, 105, 37 (SF96a)  
 Scoccimarro, R., Frieman, J., 1996b, ApJ, 473, 620 (SF96b)  
 Scoccimarro, R., Colombi, S., Fry, J.N., Frieman, J., Hivon, E., Melott, A., 1998, 496, 586  
 Zel'dovich, Ya.B., 1970. A & A, 5, 84

## APPENDIX A: CUMULANTS FROM THE LOCAL-DENSITY TRANSFORMATION OF GAUSSIAN INITIAL CONDITIONS IN LAGRANGIAN SPACE

For a generic model of non-linear evolution of the density field in which all the information is encoded in the linear density field alone, one can construct a transformation of the kind,

$$\delta = \mathcal{L}[\delta_1] = \sum_{n=1}^{\infty} \frac{c_n}{n!} [\delta_1]^n \quad (\text{A1})$$

(see Eq.[15]) with  $c_1 = 1$ , to reproduce the linear solution. This is what we shall call the *local-density* transformation. If we further assume that the above transformation describes the non-linear evolution in Lagrangian space, it has to be normalized

Next we present the general results for the cumulants including their first non-vanishing perturbative orders for GIC. For the SC model the calculation corresponds to the process described in §4. Note that this can be extended in a straightforward way to NGIC, just by taking into account the relevant terms to be kept in the perturbation series (see Paper II).

We proceed and give the coefficients of the perturbative terms according to the notation introduced in §5,

$$\begin{aligned}
 s_{2,4} &= 3 - 4c_2 + c_2^2/2 + c_3 \\
 s_{2,6} &= 15 - 36c_2 + 81c_2^2/4 - 3c_2^3/2 + 10c_3 - 7c_2c_3 \\
 &\quad + 5c_3^2/12 - 7c_4/4 + c_2c_4/2 + c_5/4 \\
 S_{3,0} &= 3c_2 \\
 S_{3,2} &= (-4 + 15c_2^2 - 4c_2^3 - 8c_3 + 3c_4)/2 \\
 S_{3,4} &= -18 + 44c_2 - 16c_2^2 - 3c_2^3 - 7c_2^4 + 5c_2^5/4 \\
 &\quad - 22c_3 + 12c_2c_3 + 10c_2^2c_3 + c_2^3c_3 - 4c_2^4 \\
 &\quad - 7c_2c_3^2/4 + 5c_4 + 9c_2c_4/8 - 9c_2^2c_4/4 \\
 &\quad + c_3c_4 - 2c_5 + 3c_2c_5/4 + 3c_6/8 \\
 S_{4,0} &= 12c_2^2 + 4c_3 \\
 S_{4,2} &= 6 - 36c_2 + 15c_2^2 + 60c_2^3 - 15c_2^4 - 4c_3 \\
 &\quad - 20c_2c_3 - 6c_2^2c_3 - 5c_4 + 18c_2c_4 + 2c_5 \\
 S_{4,4} &= (180 - 984c_2 + 1488c_2^2 - 534c_2^3 + 99c_2^4 \\
 &\quad - 180c_2^5 + 27c_2^6 + 260c_3 - 816c_2c_3 \\
 &\quad + 232c_2^2c_3 + 144c_2^3c_3 + 30c_2^4c_3 + 76c_2^5 \\
 &\quad - 48c_2c_3^2 - 30c_2^2c_3^2 - 4c_3^3 - 86c_4 \\
 &\quad + 163c_2c_4 + 129c_2^2c_4 - 66c_2^3c_4 - 72c_2c_4 \\
 &\quad + 8c_2c_3c_4 + 16c_2^2c_4 + 8c_5 - 40c_2c_5 \\
 &\quad + 12c_2^2c_5 + 7c_2c_5 - 5c_6 + 12c_2c_6 + c_7)/2 \\
 S_{5,0} &= 60c_2^3 + 60c_2c_3 + 5c_4 \\
 S_{5,2} &= -24 + 180c_2 - 510c_2^2 + 240c_2^3 + 450c_2^4 \\
 &\quad - 108c_2^5 - 80c_3 + 90c_2^2c_3 - 120c_2^3c_3 \\
 &\quad - 90c_2^4 - 10c_4 - 105c_2c_4/2 + 170c_2^2c_4 \\
 &\quad + 50c_2c_4 - 6c_5 + 40c_2c_5 + 5c_6/2 \\
 S_{6,0} &= 6(60c_2^4 + 120c_2^2c_3 + 15c_2^3 + 20c_2c_4 + c_5) \\
 S_{6,2} &= 120 - 1080c_2 + 3870c_2^2 - 6930c_2^3 + 3060c_2^4 \\
 &\quad + 3600c_2^5 - 840c_2^6 + 480c_3 - 3240c_2c_3 \\
 &\quad + 1500c_2^2c_3 + 3840c_2^3c_3 - 1800c_2^4c_3
 \end{aligned}$$

$$\begin{aligned}
& - 110c_3^2 - 1620c_2c_3^2 - 225c_2^2c_3^2 + 30c_3^3 \\
& - 150c_4 - 135c_2c_4 - 60c_2^2c_4 + 1500c_2^3c_4 \\
& - 420c_3c_4 + 1500c_2c_3c_4 + 105c_4^2 - 18c_5 \\
& - 108c_2c_5 + 585c_2^2c_5 + 135c_3c_5 - 7c_6 \\
& + 75c_2c_6 + 3c_7.
\end{aligned} \tag{A2}$$

Note that all the values of  $c_n$  can be obtained (or rewritten) in terms of the tree-level alone,  $S_{J,0}$ , indicating that the knowledge of the tree-level is enough to fully specify the underlying local-density transformation, and, therefore, to generate all higher order corrections.

Furthermore, we can make use of the general formula for the top-hat filtering derived in §4.4, and generalize the above given expressions by replacing the unsmoothed  $c_k$  coefficients by their smoothed counterparts  $\bar{c}_k$  in the following way:

$$\begin{aligned}
\bar{c}_2 &= c_2 + \frac{\gamma_1}{3} \\
\bar{c}_3 &= c_3 - \frac{\gamma_1}{2} + \frac{3}{2}c_2\gamma_1 + \frac{\gamma_1^2}{4} + \frac{\gamma_2}{6} \\
\bar{c}_4 &= c_4 + \frac{4}{3}\gamma_1 - 4c_2\gamma_1 + 2c_2^2\gamma_1 + \frac{8}{3}c_3\gamma_1 \\
& - \frac{4}{3}\gamma_1^2 + \frac{8}{3}c_2\gamma_1^2 + \frac{8}{27}\gamma_1^3 - \frac{2}{3}\gamma_2 + \frac{4}{3}c_2\gamma_2 \\
& + \frac{4}{9}\gamma_1\gamma_2 + \frac{2}{27}\gamma_3,
\end{aligned} \tag{A3}$$

and so on, where:

$$\gamma_p = \gamma_p(R) = \frac{d^p \log \hat{\sigma}_l^2}{d \log^p R}.$$

These expressions are valid for arbitrary dynamics (to be specified through the unsmoothed coefficients) and a generic initial power spectrum. They can be used for the particular cases of interest. For the SC dynamics ( $c_k = \nu_k$  as given by Eq.[37]) we find for the first coefficients of the cumulants,

$$\begin{aligned}
s_{2,4} &= \frac{1909}{1323} + \frac{143}{126}\gamma_1 + \frac{11}{36}\gamma_1^2 + \frac{\gamma_2}{6} \\
S_{3,0} &= \frac{34}{7} + \gamma_1 \\
S_{3,2} &= \frac{1026488}{101871} + \frac{12862}{1323}\gamma_1 + \frac{407}{126}\gamma_1^2 + \frac{10}{27}\gamma_1^3 \\
& + \frac{11}{7}\gamma_2 + \frac{2}{3}\gamma_1\gamma_2 + \frac{\gamma_3}{9} \\
S_{4,0} &= \frac{60712}{1323} + \frac{62}{3}\gamma_1 + \frac{7}{3}\gamma_1^2 + \frac{2}{3}\gamma_2 \\
S_{4,2} &= \frac{22336534498}{83432349} + \frac{42649448}{130977}\gamma_1 + \frac{3571621}{23814}\gamma_1^2 \\
& + \frac{35047}{1134}\gamma_1^3 + \frac{1549}{648}\gamma_1^4 + \frac{575777}{11907}\gamma_2 + \frac{5981}{189}\gamma_1\gamma_2 \\
& + \frac{263}{54}\gamma_1^2\gamma_2 + \frac{25}{54}\gamma_2^2 + \frac{2084}{567}\gamma_3 + \frac{86}{81}\gamma_1\gamma_3 + \frac{5}{81}\gamma_4
\end{aligned} \tag{A4}$$

This way, the results for the SC and SSZA dynamics described in the text (see §5 and Appendix D respectively) are given as particular cases of this *local-density* transformation in Lagrangian space whenever we replace the  $c_k$  coefficients by those associated to the relevant dynamics:  $c_k = \nu_k$  or  $c_k = \bar{\nu}_k$  for the unsmoothed or smoothed fields respectively (the previous being a particular case of the latter). The same expressions hold for the velocity divergence fields, replacing

$c_k = \mu_k$  or  $c_k = \bar{\mu}_k$  for the unsmoothed and smoothed fields respectively. These  $\mu_k$  coefficients are related to those for the density field through the equation of continuity (see Paper III for details).

## APPENDIX B: CUMULANTS FROM THE LOCAL-DENSITY TRANSFORMATION OF GAUSSIAN INITIAL CONDITIONS IN EULER SPACE

In this section we derive the cumulants from the local-density transformation of GIC in Euler space to quantify the departures from the Lagrangian formulation and give values for the SC approximation. The formulae given below reproduce those given in Fry & Gaztañaga (1993). There, they were presented as a bias transformation between the luminous and the underlying matter fluctuations. They can also be obtained by simply replacing  $F_n = c_n/n!$  in the expressions for the loop corrections (in Euler space) given in SF96a.

The first perturbative contributions to the cumulants in Euler space are the following,

$$\begin{aligned}
s_{2,4} &= \frac{c_2^2}{2} + c_3 \\
\xi_{3,6} &= c_2^3 + 6c_2c_3 + \frac{3}{2}c_4 \\
S_{3,0} &= 3c_2 \\
S_{3,2} &= -2c_2^3 + \frac{3}{2}c_4 \\
S_{4,0} &= 12c_2^2 + 4c_3 \\
S_{4,2} &= -15c_2^4 - 6c_2^2c_3 + 18c_2c_4 + 2c_5.
\end{aligned} \tag{B1}$$

where we have also computed the third order cumulant,  $\xi_3$  whose one-loop contribution is denoted by  $\xi_{3,6}$  following the notation introduced in §5. It is easy to see that this contribution is given by  $\xi_{3,6} = S_{3,2} + 2s_{2,4}S_{3,0}$ .

Replacing in these expressions the values for the SC dynamics with a top-hat filter and a power-law spectrum, *i.e.*, introducing the smoothed coefficients given by Eqs.[47],[37], we get estimates for the cumulants as summarized in Table B1. For a comparison of both the Lagrangian and Eulerian predictions within the SC model with respect to the exact PT values we also display the results by SF96a, SF96b and S97 obtained using the diagrammatic representation for PT.

Notice that unlike the case for the SC estimates from Lagrangian space, the Euler estimates just give the right order of magnitude for the cumulants when compared against exact analytic calculations (see Eqs.[53], [55]). The observed trend is that (non-reduced) cumulants in Euler space typically overestimate those in Lagrangian space as the normalization factor (see Eq.[39]) between the two spaces introduces terms that give a negative *non-local* net contribution in terms of the variance (see §5.1 for a discussion).

Since this overestimation effect in the higher-order cumulants scales less steeply than hierarchically with respect to that of the variance,  $\Delta\xi_J \lesssim (\Delta\xi_2)^{J-1}$ , the effect in the  $S_J$  ratios is thus dominated by that in the variance. This results in a net underestimate of the  $S_J$  ratios. Notice that the relative underestimation becomes larger and larger as smoothing effects increase.

| SC               | Unsmoothed   | Smoothed      |               |               |
|------------------|--------------|---------------|---------------|---------------|
|                  | $\gamma = 0$ | $\gamma = -1$ | $\gamma = -2$ | $\gamma = -3$ |
|                  | $n = -3$     | $n = -2$      | $n = -1$      | $n = 0$       |
| $s_{2,4}^E$      | 4.92         | 2.76          | 1.20          | 0.26          |
| $s_{2,4}^L$      | 1.44         | 0.61          | 0.40          | 0.79          |
| $s_{2,4}^{PT}$   | 1.82         | 0.88          | ?             | ?             |
| $\xi_{3,6}^E$    | 54.64        | 21.80         | 5.68          | 0.38          |
| $\xi_{3,6}^L$    | 24.09        | 7.95          | 2.85          | 2.91          |
| $\xi_{3,6}^{PT}$ | 27.49        | 9.97          | ?             | ?             |
| $S_{3,2}^E$      | 6.85         | 0.54          | -1.21         | -0.60         |
| $S_{3,2}^L$      | 10.08        | 3.21          | 0.59          | -0.02         |
| $S_{3,2}^{PT}$   | 9.80         | 3.18          | ?             | ?             |
| $S_{4,2}^E$      | 208.45       | 24.83         | -10.71        | -3.09         |
| $S_{4,2}^L$      | 267.72       | 63.56         | 7.39          | -0.16         |
| $S_{4,2}^{PT}$   | ?            | ?             | ?             | ?             |

**Table B1.** Comparison between the cumulants in the SC model in Euler space ( $E$ ) with those in Lagrangian space ( $L$ ) and in exact PT ( $PT$ ).

### APPENDIX C: TOP-HAT SMOOTHING IN FOURIER SPACE

To illustrate the fact that the SC model gives the correct smoothed tree-level amplitudes for Gaussian initial conditions for a top-hat window, we shall derive  $\overline{\nu_2}$  explicitly by imposing the *spherically symmetric* approximation in Fourier space and show that the skewness  $S_3 = 3\overline{\nu_2}$ , exactly reproduces the leading order exact perturbative result, Eq.[47]: *e.g.*,  $\overline{\nu_2} = \nu_2 + \gamma/3$ . We perform the calculation in Euler space but the result does not differ from that in Lagrangian space at tree-level for Gaussian initial conditions, as discussed in §4. Differences are only expected to appear in higher perturbative orders ( $\sigma$ -corrections).

To see this, we recall the properties derived by Bernardeau 1994b (B94b henceforth) for a top-hat window function (spherical window) defined as,

$$W_{TH}(\mathbf{x}) = 1 \quad \text{if } |\mathbf{x}| \leq R_0,$$

and 0 otherwise, for a scale  $R_0$ , so that the smoothed fields are obtained through the integral,

$$\overline{\delta} \equiv \delta(R_0) = \int d^3\mathbf{x} W_{TH}(\mathbf{x}) \delta(\mathbf{x}),$$

We turn to Fourier space for convenience, where the smoothed fields are expressed as,

$$\delta(R_0) = \int \frac{d^3\mathbf{k}}{(2\pi)^{3/2}} W_{TH}(\mathbf{k}R_0) \delta(\mathbf{k}),$$

where  $W_{TH}(\mathbf{k}R_0)$  is the Fourier transform of  $W_{TH}(\mathbf{x})$ . In

particular, for the second-order in the perturbative series, we have for the smoothed field

$$\delta_2(R_0) = \int \frac{d^3\mathbf{k}_1}{(2\pi)^{3/2}} \frac{d^3\mathbf{k}_2}{(2\pi)^{3/2}} \delta_{\mathbf{k}_1} \delta_{\mathbf{k}_2} W(|\mathbf{k}_1 + \mathbf{k}_2| R_0) \\ \times \left[ D_1^2 \left( P_{1,2} - \frac{3}{2} Q_{1,2} \right) + \frac{3}{4} D_2 Q_{1,2} \right],$$

where,

$$P_{1,2} = 1 + \frac{\mathbf{k}_1 \cdot \mathbf{k}_2}{k_1^2}, \quad Q_{1,2} = 1 + \frac{(\mathbf{k}_1 \cdot \mathbf{k}_2)^2}{k_1^2 k_2^2},$$

and  $D_i$  are the time-dependent growth factors for the  $i$ -th perturbative order to be solved with the SC equations of motion. Now, decomposing the integrals into their angular and radial part and translating the property of spherical symmetry into Fourier space language,

$$\delta_{\mathbf{k}_i} = \delta_{|\mathbf{k}_i|}, \quad (C1)$$

we can apply some properties for the top-hat window function (see B94b, Eqs.[A5] and [A6]) and get,

$$\delta_2(R_0) = \left( \frac{D_2}{2D_1^2} + \frac{1}{6} \frac{d \log[\delta_l(R_0)]^2}{d \log R_0} \right) [\delta_l(R_0)]^2,$$

since,

$$\delta_l(R_0) = \int \frac{d^3\mathbf{k}}{(2\pi)^{3/2}} W_{TH}(\mathbf{k}R_0) \delta_{\mathbf{k}} D_1(t).$$

We further use the fact that in general the smoothed linear density contrast at a point  $x$ , can be factorized in its scale dependent part  $\sigma(R_0)$  and its normalized linear field  $\varepsilon(x)$ ,  $\delta_l(R_0) \equiv \delta_l(R_0, x) = \sigma_l(R_0) \eta(x)$ , and we finally get:

$$\delta_2(R_0) = \frac{1}{2} \left( \frac{34}{21} + \frac{1}{3} \frac{d \log[\sigma_l(R_0)]^2}{d \log R_0} \right) [\delta_l(R_0)]^2. \quad (C2)$$

If we define,  $\delta_2(R_0) \equiv (\overline{\nu_2}/2) [\delta_l(R_0)]^2$ , we find

$$\overline{\nu_2} = \frac{34}{21} + \frac{1}{3} \frac{d \log[\sigma_l(R_0)]^2}{d \log R_0} = \nu_2 + \frac{\gamma}{3} \quad (C3)$$

which exactly reproduces Eq.[47]. This result can be extended to higher orders following the properties of the top-hat window presented in B94b.

### APPENDIX D: THE SPHERICALLY SYMMETRIC ZEL'DOVICH APPROXIMATION

A simple accurate description of the non-linear dynamics of the fluid elements before shell crossing (single streaming regime) is provided by the so-called Zel'dovich approximation (hereafter ZA, see Zel'dovich 1970). According to this approximation, particle positions in comoving coordinates are assumed to follow straight lines. Despite being exact only at linear order in Lagrangian PT, the latter solution has been successfully tested as an accurate approximation for the description of the dynamics in the non-linear regime (see *e.g.*, Croft & Gaztañaga 1998). Within the ZA the fluid equations can then be easily integrated, and yield

$$1 + \delta = \prod_{i=1}^N \frac{1}{(1 - D(t) \lambda_i)}, \quad (D1)$$

where  $N$  is the number of spatial dimensions and  $\lambda_i = -\partial\psi_i/\partial q_i$ , which is in general a *non-local* relation between the displacement field and the evolved density fluctuation.

At this point we introduce the *spherically symmetric* assumption for the ZA dynamics (SSZA) as we did before with the exact dynamics. Thus we set  $\lambda_i = \lambda$ , *i.e.*, all directional derivatives are equal due to the spherical symmetry (no tidal forces) and rewrite,  $\delta_l = D(t) \sum_{i=1}^N \lambda_i = 3 D(t) \lambda$ , as follows from linearising Eq.[D1]. The assumption of spherical symmetry renders the relation Eq.[D1] as a local transformation that may be expanded in power series to get the full perturbative series for the density contrast. In particular, for the 3D case, the normalized SSZA transformation has the form,

$$\delta \sim (1 - \delta_l/3)^{-3}, \quad (\text{D2})$$

to be normalized according to Eq.[39]. Notice that the latter transformation may be straightforwardly extended to any spatial dimensions. As seen in Fosalba *et al.* (1998), the exponential transformation that leads to the lognormal hierarchical amplitudes,  $S_J = J^{J-2}$ , are only recovered when one takes the limit of infinite spatial dimensions (see also Bernardeau and Kofman 1995), which does not make much physical sense.

Expanding Eq.[D2] in power series we can determine the unsmoothed coefficients  $\nu_k$  of the local non-linear transformation for the SSZA,

$$\begin{aligned} \nu_2 &= \frac{4}{3} \sim 1.33; \quad \nu_3 = \frac{20}{9} \sim 2.22 \\ \nu_4 &= \frac{40}{9} \sim 4.44; \quad \nu_5 = \frac{280}{27} \sim 10.37, \end{aligned} \quad (\text{D3})$$

and so forth. Introducing them in the smoothed transformation according to Eq.[47] for a top-hat window, we can now find, using Eq.[A3] with  $c_k = \overline{\nu_k}$ , the following results for the smoothed density field for GIC, and a power-law power spectrum,

$$\begin{aligned} s_{2,4} &= \frac{7}{9} + \frac{11}{18} \gamma + \frac{11}{36} \gamma^2 \\ s_{2,6} &= \frac{185}{243} + \frac{535}{324} \gamma + \frac{1043}{648} \gamma^2 + \frac{127}{162} \gamma^3 + \frac{127}{648} \gamma^4 \\ S_{3,0} &\equiv S_3^{(0)} = 4 + \gamma \\ S_{3,2} &= \frac{118}{27} + \frac{16}{3} \gamma + \frac{41}{18} \gamma^2 + \frac{10}{27} \gamma^3 \\ S_{4,0} &\equiv S_4^{(0)} = \frac{272}{9} + \frac{50}{3} \gamma + \frac{7}{3} \gamma^2 \\ S_{4,2} &= \frac{2506}{27} + \frac{11512}{81} \gamma + \frac{13523}{162} \gamma^2 + \frac{3679}{162} \gamma^3 + \frac{1549}{648} \gamma^4 \end{aligned} \quad (\text{D4})$$

The results for the variance and  $S_J$  for the SSZA for particular values of the spectral index are given in Table D1.

For the *unsmoothed* fields ( $\gamma = 0$ ), analytic results including the two corrective terms beyond the tree-level, were derived by SF96a in the context of the diagrammatic approach. For the variance, skewness, and the kurtosis (the latter only up to the first  $\sigma$ -correction) they give,

$$\begin{aligned} \sigma^2 &\approx \sigma_l^2 + 1.27 \sigma_l^4 + 2.02 \sigma_l^6 + \mathcal{O}(\sigma_l^8) \\ S_3 &\approx 4 + 4.69 \sigma_l^2 + 13.93 \sigma_l^4 + \mathcal{O}(\sigma_l^6) \\ S_4 &\approx 30.22 + 98.51 \sigma_l^2 + \mathcal{O}(\sigma_l^4). \end{aligned} \quad (\text{D5})$$

| SSZA      | Unsmoothed   |               | Smoothed      |               |
|-----------|--------------|---------------|---------------|---------------|
|           | $\gamma = 0$ | $\gamma = -1$ | $\gamma = -2$ | $\gamma = -3$ |
|           | $n = -3$     | $n = -2$      | $n = -1$      | $n = 0$       |
| $s_{2,4}$ | 0.78         | 0.47          | 0.78          | 1.69          |
| $S_{3,0}$ | 4            | 3             | 2             | 1             |
| $S_{3,2}$ | 4.37         | 0.94          | -0.15         | -1.13         |
| $S_{4,0}$ | 30.22        | 15.89         | 6.22          | 1.22          |
| $S_{4,2}$ | 92.81        | 13.85         | -0.96         | -1.82         |

**Table D1.** Values for the higher-order perturbative contributions for the SSZA for the unsmoothed ( $n = -3$ ) and smoothed ( $n = -2, -1, 0$ ) density fields, for a top-hat window and a power-law power spectrum.

These results are to be compared to our results from the SC model in the perturbative regime (truncated at the same order),

$$\begin{aligned} \sigma^2 &\approx \sigma_l^2 + 0.78 \sigma_l^4 + 0.76 \sigma_l^6 + \mathcal{O}(\sigma_l^8) \\ S_3 &\approx 4 + 4.37 \sigma_l^2 + 9.41 \sigma_l^4 + \mathcal{O}(\sigma_l^6) \\ S_4 &\approx 30.22 + 92.81 \sigma_l^2 + 331.0 \sigma_l^4 + \mathcal{O}(\sigma_l^6), \end{aligned} \quad (\text{D6})$$

which differ in 7% in the corrective term for  $S_3$ , 6% in the corrective term for  $S_4$ , and up to 40% in the one-loop term for the variance. The two-loop contributions for  $S_3$  differ in about 30% and just give the right order of magnitude for the variance. The two-loop contribution to  $S_4$  ( $\sim 331 \sigma_l^2$ ) must be taken just as an estimate of the actual value for this coefficient in PT, since there are no analytic results available to compare to. All the above quoted differences must be attributed to the tidal effects as argued before what gives further support to the view that the hierarchical amplitudes are essentially of a *shearless* nature unlike the (unreduced) one-point cumulants.

For the smoothed density field in the ZA to PT there is only one result available concerning the skewness for  $n = -2$  (see S97),

$$S_3 \approx 3 + 0.82 \sigma_l^2 + \mathcal{O}(\sigma_l^4), \quad (\text{D7})$$

while within the SSZA dynamics, we obtain,

$$S_3 \approx 3 + 0.94 \sigma_l^2 + \mathcal{O}(\sigma_l^4), \quad (\text{D8})$$

which means a 15% negative contribution from the shear for the first corrective term for that particular value of the spectral index.

In Fig D1 we display the deviations from the tree-level values for the variance, skewness and kurtosis for the SSZA up to 2nd perturbative contribution (one-loop). In line with the arguments pointed out for the spherically symmetric approximation to the exact PT (the SC model), here the smoothing effects tend to diminish the non-linear corrections as well. We have checked that the 3rd order contribution follows qualitatively the same behavior although non-linearities are typically larger. On the other hand, the lack of a critical index (vanishing non-linearities) for the variance gives further support to our claim that it is due to the

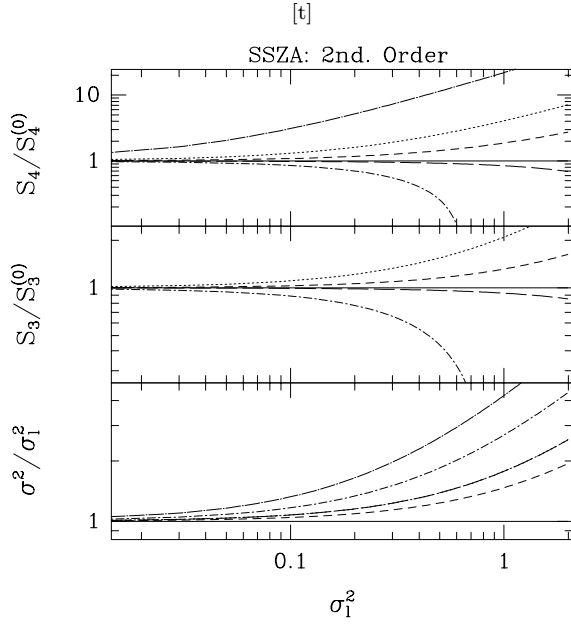


**Figure D1.** Same as Fig 1, for the SSZA. In this case, the variance has a minimum corrective term for  $n \approx -1$ , and the hierarchical amplitudes show a vanishing first corrective term for  $n \approx -1.2$ . Notice that the  $n = 1$  line is not plotted for the skewness since for that particular value the tree-level exactly vanishes.

local nature of the SC picture and thus, to the loss of the previrialization effect.